

# The architecture of information processing in biological systems

Giorgio Nicoletti,<sup>1,2,3</sup> Matteo Bruzzone,<sup>4,5</sup> Samir Suweis,<sup>1,5</sup> Marco Dal Maschio,<sup>4,5</sup> and Daniel Maria Busiello<sup>3</sup>

<sup>1</sup>*Laboratory of Interdisciplinary Physics, Department of Physics and Astronomy “Galileo Galilei”, University of Padova, Padova, Italy*

<sup>2</sup>*Department of Mathematics “Tullio Levi-Civita”, University of Padova, Padova, Italy*

<sup>3</sup>*Max Planck Institute for the Physics of Complex Systems, Dresden, Germany*

<sup>4</sup>*Department of Biomedical Science, University of Padova, Padova, Italy*

<sup>5</sup>*Padova Neuroscience Center, University of Padova, Padova, Italy*

Biological systems process information at different scales and adapt to their changing environment. Informed both by experimental observations and theoretical constraints, we propose a chemical model for sensing that incorporates energy consumption, information storage, and negative feedback. We show that a biochemical architecture enclosing these minimal mechanisms leads to the emergence of dynamical memory and adaptation. Crucially, adaptation is associated with both an increase in the mutual information between external and internal variables and a reduction of dissipation of the internal chemical processes. By simultaneously minimizing energy consumption and maximizing information, we find that far-from-equilibrium sensing dominates in the low-noise regime. Our results, in principle, can be declined at different biological scales. We employ our model to shed light on large-scale neural adaptation in zebrafish larvae under repeated visual stimulation. We find striking similarities between predicted and observed behaviors, capturing the emergent adaptation of neural response. Our framework draws a path toward the unraveling of the essential ingredients that connect information processing, adaptation, and memory in biological systems.

Sensing and adaptation mechanisms in biological systems span a wide range of temporal and spatial scales, from cellular to multi-cellular level, forming a basis for decision-making and the optimization of limited resources [1–8]. Prominent examples include the modulation of flagellar motion operated by bacteria according to changes in the local nutrient concentration [9–11], the regulation of immune responses through feedback mechanisms [12, 13], and the maintenance of high sensitivity in varying environments for olfactory and visual sensing in mammalian neurons [14–18].

In the last decade, advances in experimental techniques fostered the quest for the core biochemical mechanisms governing information processing. Simultaneous recordings of hundreds of biological signals made it possible to infer distinctive features directly from data [19–22]. However, many approaches fall short of describing the connection between the underlying chemical processes and the observed behaviors [23–26]. As a step in this direction, a multitude of works focused on the architecture of specific signaling networks, from tumor necrosis factor [12, 13] to chemotaxis [9, 27], highlighting the essential structural ingredients for their efficient functioning. An observation shared by the majority of these studies is the key role of a negative feedback mechanism to induce an emergent adaptive response [28–31].

Moreover, information-thermodynamic laws prescribe the necessity of a storage mechanism for any information-processing device [32], an unavoidable feature compatible with the structure of numerous chemical signaling networks [9, 28]. The storage of information is also accountable for energy consumption during processing [33, 34], as chemical sensing has to take place out-of-equilibrium [3, 35–37]. Furthermore, the recent discovery of memory molecules in different contexts [38–40] hints at the onset

of a finite-time memory at a molecular scale that dynamically builds up information. Although several models have been proposed mostly in specific contexts [9, 27, 41], a minimal but comprehensive framework that describes the role of information storage in shaping sensing and adaptation dynamics in biological systems remains elusive.

In this work, we present an archetypal model for sensing that starts from a thermodynamically consistent description of its underlying chemical processes. Our framework describes the coupled dynamics of a receptor, a readout population, and a storage population. These minimal ingredients explicitly incorporate energy consumption, information storage, and negative feedback, in agreement with the aforementioned experimental observations and theoretical constraints. We show that the combined effects of storage and negative feedback promote the emergence of a rich information dynamics shaped by adaptation and finite-time memory. In particular, the storage mechanism acts as a chemical information reservoir for the system, allowing it to dynamically build up information on an external environment while reducing internal dissipation. Optimal sensing emerges from a dissipation-information trade-off, revealing the importance of far-from-equilibrium conditions in low-noise regimes. Remarkably, the proposed biochemical architecture is capable of capturing the diverse and complex sensing mechanisms that operate within biological systems at multiple scales. In particular, adaptation is a frequent phenomenon that characterizes many neuronal circuits along the sensory-motor processing pathways in most living organisms, either invertebrates or vertebrates [42–44]. Therefore, we test our model at the mesoscopic scale of neural responses of zebrafish larvae subjected to repeated visual stimuli.

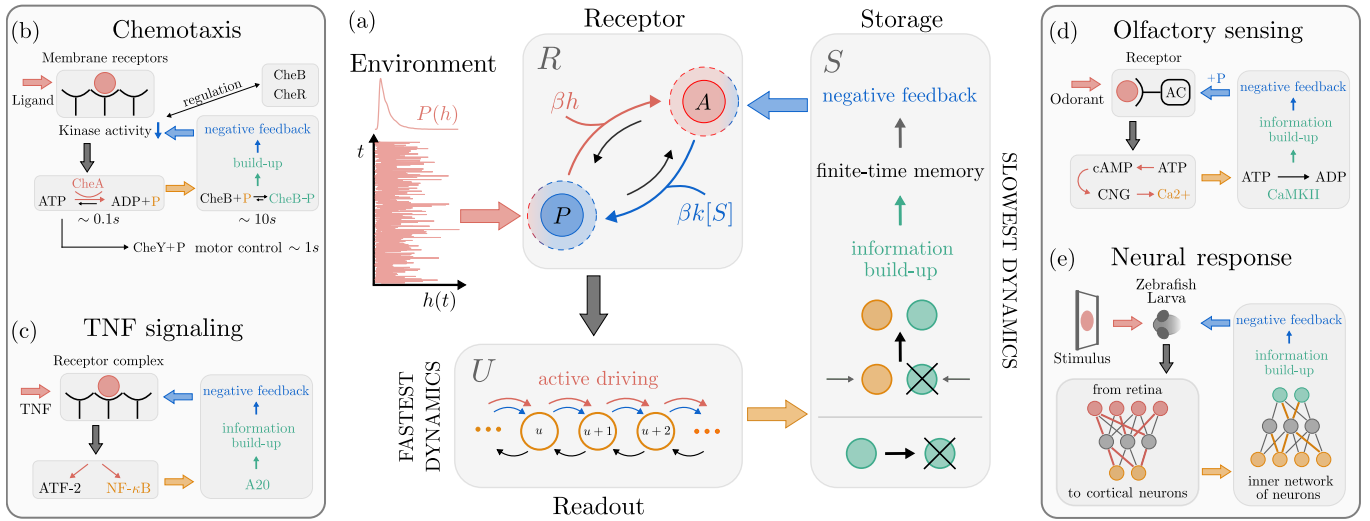


FIG. 1. Sketch of the model architecture and biological examples at different scales. (a) A receptor  $R$  can be either in an active ( $A$ ) or passive ( $P$ ) state, with transitions following two pathways, one used for sensing (red) and affected by the environment  $h$ , and the other (blue) modified by the storage concentration,  $[S]$ . An active receptor increases the response of a readout population  $U$  (orange), which in turns stimulates the production of storage molecules  $S$  (green) that provide a negative feedback to the receptor. (b) In chemotaxis, the input ligand binds to membrane receptors, regulating motor control and producing phosphate groups, whose concentration regulates the receptor methylation level. (c) Similarly, in tumor necrosis factor (TNF) signaling the nuclear factor  $NF - \kappa B$  is produced after receptor binding to TNF.  $NF - \kappa B$  modulates the encoding of the zinc-finger protein A20, which closes the feedback loop by inhibiting the receptor complex. (d) In olfactory sensing, odorant binding induces the activation of adenylyl cyclase (AC). AC stimulates a calcium flux, eventually producing phosphorylase calmodulin kinase II (CAMKII) which phosphorylates and deactivates AC. (e) In neural response, multiple mechanisms may take place at different scales. In zebrafish larvae, visual stimulation is projected along the visual stream from the retina to the cortex, a coarse-grained realization of the  $R$ - $U$  dynamics. Inhibitory populations and molecular mechanisms, such as short-term synaptic depotentiation, are responsible for an adapted response upon repeated stimulation.

### Storage and feedback in dissipative chemical sensing

We describe a receptor  $R$  that can be either active ( $r = 1$ ) or passive ( $r = 0$ ), with the two states separated by an energetic barrier  $\Delta E = E_A - E_P > 0$  (Figure 1a). The receptor undergoes spontaneous transitions between the passive and active states and it is stimulated by an external signal  $h(t)$ , the input to be encoded by the system. The environment, described by a time-dependent probability distribution  $p_H(h, t)$ , acts as a non-equilibrium energetic driving that favors activation. Conversely, inhibition takes place through a negative feedback process mediated by the concentration of a chemical population  $S$ . Its role is to store information about the external signal and use it to limit further activation of the sensing network.

Activation triggered by the environmental signal acts along a “sensing pathway” (superscript  $H$ ), while the inhibition mechanism affects the “internal pathway” (superscript  $I$ ) between the receptor’s states. This choice represents a coarse-grained description of the different chemical networks that realize these two processes. Reaction rates follow the standard Arrhenius’ law:

$$\begin{aligned} \Gamma_{P \rightarrow A}^{(H)} &= e^{\beta(h - \Delta E)} \Gamma_H^0 & \Gamma_{A \rightarrow P}^{(H)} &= \Gamma_H^0 \\ \Gamma_{P \rightarrow A}^{(I)} &= e^{-\beta \Delta E} \Gamma_I^0 & \Gamma_{A \rightarrow P}^{(I)} &= \Gamma_I^0 e^{\beta z(s/N_S)} \end{aligned} \quad (1)$$

where  $\Gamma_H^0$  and  $\Gamma_I^0$  set the time-scales of the two pathways. Chemical inhibition of the receptor,  $\Gamma_{A \rightarrow P}^{(I)}$ , depends on the concentration of  $S$  at a given time through a function  $z(s/N_S)$ , where  $N_S$  is the maximum number of storage molecules available. Crucially, the presence of two different transition pathways creates an internal non-equilibrium cycle in receptor dynamics (see Methods).

The receptor actively drives the production of a readout population  $U$ , e.g., phosphate molecules for chemotactic response [9, 27], the nuclear factor in TNF signaling networks [12, 13], calcium for olfactory sensing mechanisms [14, 15], or photoreceptors for visual sensing [16–18] (Figures 1b-e). In full generality, we model the dynamics of both readout and storage populations with chemical master equations. In particular, the dynamics of  $U$  is given by:

$$\begin{aligned} \emptyset_U \rightarrow U & & U \rightarrow \emptyset_U & & (2) \\ \Gamma_{u \rightarrow u+1} &= e^{-\beta(V - cr)} \Gamma_U^0 & \Gamma_{u+1 \rightarrow u} &= (u+1) \Gamma_U^0 \end{aligned}$$

where  $u$  denotes the number of molecules,  $V$  is the energy needed to produce a readout unit,  $c$  the receptor-induced driving, and  $\Gamma_U^0$  sets the process timescale. Hence, active receptors transduce the environmental energy into an active pumping on the readout node, allowing readout molecules to encode information on the external signal.

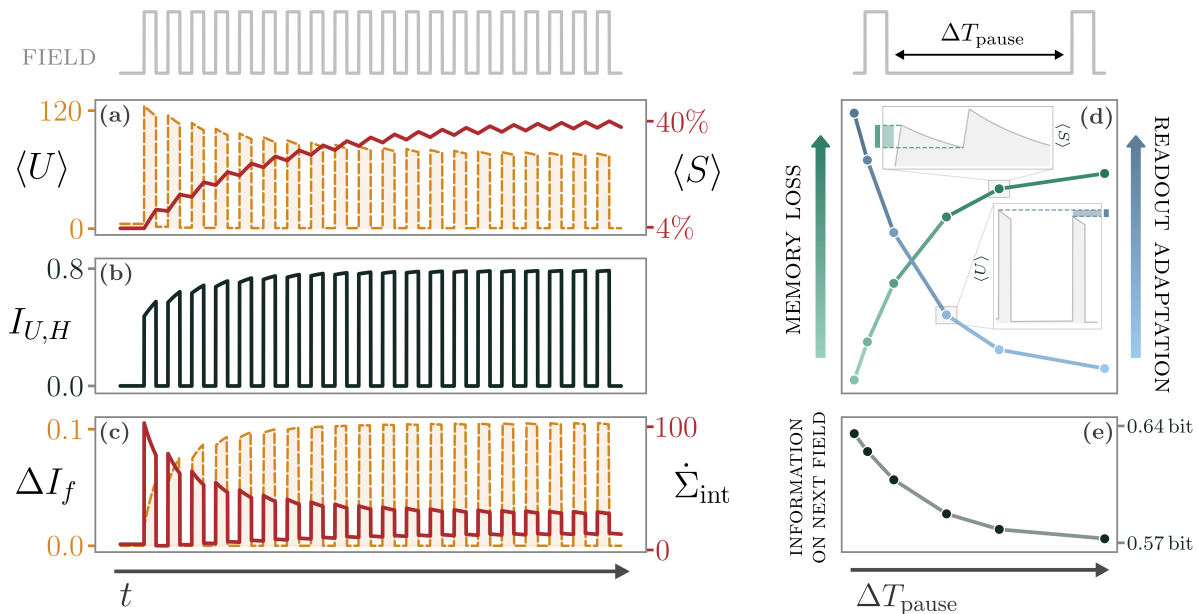
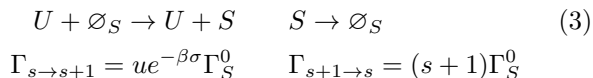


FIG. 2. Evolution of the model under a switching external field  $H$ . (a) The average readout population  $\langle U \rangle$  (orange) decreases with the number of repetitions, adapting as a consequence of the negative feedback from the storage population, whose average  $\langle S \rangle$  (red) increases in time. At large times, the system reaches a periodic steady state. (b) Adaptation can be understood in terms of information that the system encodes on  $H$  through the readout,  $I_{U,H}$ , which increases with the repetitions and is maximized at long times. (c) The information feedback between  $U$  and  $S$ ,  $\Delta I_f$  (orange), increases with time, indicating that the negative feedback drives the adapted response due to the stored information. At the same time, the entropy production  $\dot{\Sigma}_{\text{int}}$  (red) decreases with adaptation. (d) The system response depends on the waiting time  $\Delta T_{\text{pause}}$  between two external signals. As  $\Delta T_{\text{pause}}$  increases, the dynamical storage decays and thus memory is lost (green), whereas the adaptation of the readout population decreases (blue). (e) As a consequence, the information  $I_{U,H}$  that the system has on the field  $H$  decays as well. Model parameters for this figure are  $\beta = 2.5$ ,  $\sigma = 0.5$ , and as specified in the Methods.

In turn, readout units catalyze the production of a storage population  $S$ , whose number of molecules  $s$  is described by:



where  $\sigma$  is the energetic cost of a storage unit,  $\Gamma_S^0$  sets its timescale, and  $s = N_S$  is a reflective boundary. A depletion of readout molecules by storage production will not change the results, since, as we will see, the dynamics of  $U$  is the fastest one.  $S$  may model phosphorylated methylesterase (CheB-P) in chemotactic networks [27], the zinc-finger protein in TNF signaling [12], memory molecules sensitive to calcium activity [38], and synaptic depotentiation, or, at a more coarse-grained scale, neural populations that regulate neuronal response (Figure 1b-e). Storage molecules, as we will see, are responsible for encoding the readout response and play the role of a finite-time memory. For simplicity, in Eq. (1) we choose  $z(s/N_S) = \kappa \sigma s / N_S$ , where  $\kappa$  is a proportionality constant that sets the inhibition strength.

In the complete biochemical architecture (Figure 1a), four different timescales are at play, one for receptors,  $\tau_R$ , one for the readout,  $\tau_U$ , one for the storage,  $\tau_S$ , and

another for the environment,  $\tau_H$ . We employ the biologically plausible assumption that  $U$  undergoes the fastest evolution, while  $S$  and  $H$  are the slowest degrees of freedom [27, 41], i.e.,  $\tau_U \ll \tau_R \ll \tau_S \sim \tau_H$ .

#### Adaptation and memory shape dissipation and information dynamics

The system dynamics is governed by four different operators,  $\hat{W}_X$ , with  $X = R, U, S, H$ , one for each chemical species, and one for the external field. The resulting master equation is:

$$\partial_t P = \left[ \frac{\hat{W}_R(s, h)}{\tau_R} + \frac{\hat{W}_U(r)}{\tau_U} + \frac{\hat{W}_S(u)}{\tau_S} + \frac{\hat{W}_H(h)}{\tau_H} \right] P, \quad (4)$$

where  $P$  denotes, in general, the joint propagator  $P(u, r, s, h, t | u_0, r_0, s_0, h_0, t_0)$ , with  $u_0, r_0, s_0$  and  $h_0$  initial conditions at time  $t_0$ . The intrinsic time-scale separation of our model allows us to solve self-consistently Eq. (4) (see Methods and Supplementary Information).

To investigate the features and advantages of an adaptive response, we first study the behavior of the system under a periodic switching signal with an appropriate

choice of parameters (see Methods). Although the presented results are robust, in the next section we characterize the region of feasible parameters using an optimization approach. To maintain analytical tractability, we choose  $p_H(h, t) \sim e^{-\lambda(t)h}$ , where  $\lambda(t)$  is a square wave, so that the average field  $\langle H \rangle$  switches between two values  $\langle H \rangle_{\max}$  and  $\langle H \rangle_{\min}$ . In Figure 2a we show that, as expected, the average readout population,  $\langle U \rangle$ , decreases in time, adapting the response of the system to a repeated statistically identical input. This is a direct consequence of the increase of the average storage population,  $\langle S \rangle$ , which inhibits receptor activation. Notice that a mean-field relation between  $\langle U \rangle$  and  $\langle S \rangle / N_S$  allows us to consider only the percentage of storage molecules as a relevant parameter (see Supplementary Information).

Figure 2b reveals a surprising feature. Despite a reduction in the readout population, the mutual information between  $U$  and  $H$ ,  $I_{U,H}$ , increases in time. Hence, adaptation is fostering the encoding of external information in the system response. We can understand this result as a decrease in time of the Shannon entropy of the readout population due to repeated measurements of the signal:

$$\Delta \mathcal{S}_U = k_B (\mathcal{H}_{U|H} - \mathcal{H}_U) = -k_B I_{U,H} \quad (5)$$

where  $\mathcal{H}_X$  is the Shannon entropy of  $X$ . This behavior is tightly related to the storage  $S$ , which acts as an information reservoir for the system. Indeed, if we consider that also  $S$  contains information about the signal, we have that  $\Delta \mathcal{S}_{U,S} < \Delta \mathcal{S}_U$  and thus  $\Delta I_f = I_{(U,S),H} - I_{U,H} > 0$ . Crucially,  $\Delta I_f$  increases in time (Figure 2c). We name  $\Delta I_f$  the feedback information, i.e., the net gain of information when considering how much information  $U$  and  $S$  together share with the signal. See Supplementary Information for a detailed information-theoretic analysis.

These features come along with another intriguing result. The dissipation due to the chemical processes associated with the production of  $U$  and  $S$ ,  $\dot{\Sigma}_{\text{int}}$ , decreases in time (see Methods and Figure 2c). This highlights a fundamental thermodynamic advantage of adaptation and information storage. After a large enough number of repetitions, the system has encoded the maximum amount of information on the environment and reaches a time-periodic steady state. This is characterized by adapted readout and storage concentration.

Additionally, these dynamical features reveal the emergence of a finite-time memory, which governs readout adaptation and coincides with the storage relaxation timescale. In Figure 2d, we show that the more  $\langle S \rangle$  relaxes between two consecutive signals, the less the readout population adapts to repeated stimuli. Such a concerted behavior ascribes to the storage population the role of an effective chemical memory. As a consequence, the mutual information  $I_{U,H}$  on the next field decreases as well, and the system needs to activate a larger number of  $\langle U \rangle$  (Figure 2e).

Overall, our framework captures the minimal ingredients from which adaptation to external environments

and finite-time memory arise. They lead to a twofold advantage of adaptive responses, i.e., increasing information on the input signal and reducing internal dissipation. Remarkably, removing any of the chemical populations introduced here will result into a loss of the adaptation dynamics. In particular, in the Supplementary Information, we show that information storage is necessary and necessarily slow. Let us note that the proposed model is chemical and Markovian - hence, these features are solely emerging from the combined influence of negative feedback and information storage.

### Optimal sensing as information-dissipation trade-off

In the presence of a constant external field, the receptor is driven out of equilibrium and dissipates energy, while the system acquires and stores information on the signal until it reaches a stationary state. Yet, depending on its parameters, it may or may not be successful in performing these tasks. We focus on two relevant parameters:  $\beta$ , which quantifies the thermal noise strength, and  $\sigma$ , the energetic cost of building a chemical memory. We seek for the values of  $\beta$  and  $\sigma$  that, at stationarity, maximize the information processing capability of the system, i.e.,  $I_{U,H}$  and  $\Delta I_f$ , while minimizing the dissipation of the receptor per unit temperature:

$$\delta Q_R = \left\langle \log \left( \frac{\Gamma_{P \rightarrow A}^{(H)} \Gamma_{A \rightarrow P}^{(I)}}{\Gamma_{A \rightarrow P}^{(H)} \Gamma_{P \rightarrow A}^{(I)}} \right) \right\rangle = \beta \left( \langle H \rangle + \kappa \sigma \frac{\langle S \rangle}{N_S} \right). \quad (6)$$

The result is a Pareto-like surface in the  $(I_{U,H}, \Delta I_f, -\delta Q_R)$  space, shown in Figure 3a (see Methods). In the high-noise regime (small  $\beta$ ), optimal sensing is found at a large energetic cost  $\sigma$ , as the creation of storage molecules due to strong thermal fluctuations has to be prevented. In this case, information processing is not particularly effective, i.e., mutual and feedback information are small, but the system operates in close-to-equilibrium conditions. Conversely, the low-noise regime (large  $\beta$ ) is characterized by far-from-equilibrium sensing. As thermal fluctuations are almost negligible, a small energetic cost of storage allows the system to be more sensitive to the external signal. Therefore,  $I_{U,H}$  and  $\Delta I_f$  reach higher values (see Figures 3b-d). This trade-off between information and dissipation reflects in a balanced production of readout and storage molecules, emphasizing the importance of both populations in the model, as shown in Figure 2e. See Supplementary Information for a detailed discussion of the role of thermal noise and signal strength.

However, how adaptation is related to the features of optimal sensing cannot be straightforwardly deduced from the above analysis. Indeed, adaptation is a sheer dynamical quantity, while optimal parameter choices have been explored in a stationary regime. Thus, we focus again on a switching signal as in Figure 1a-c. Adaptation efficacy is quantified through the net increase in readout

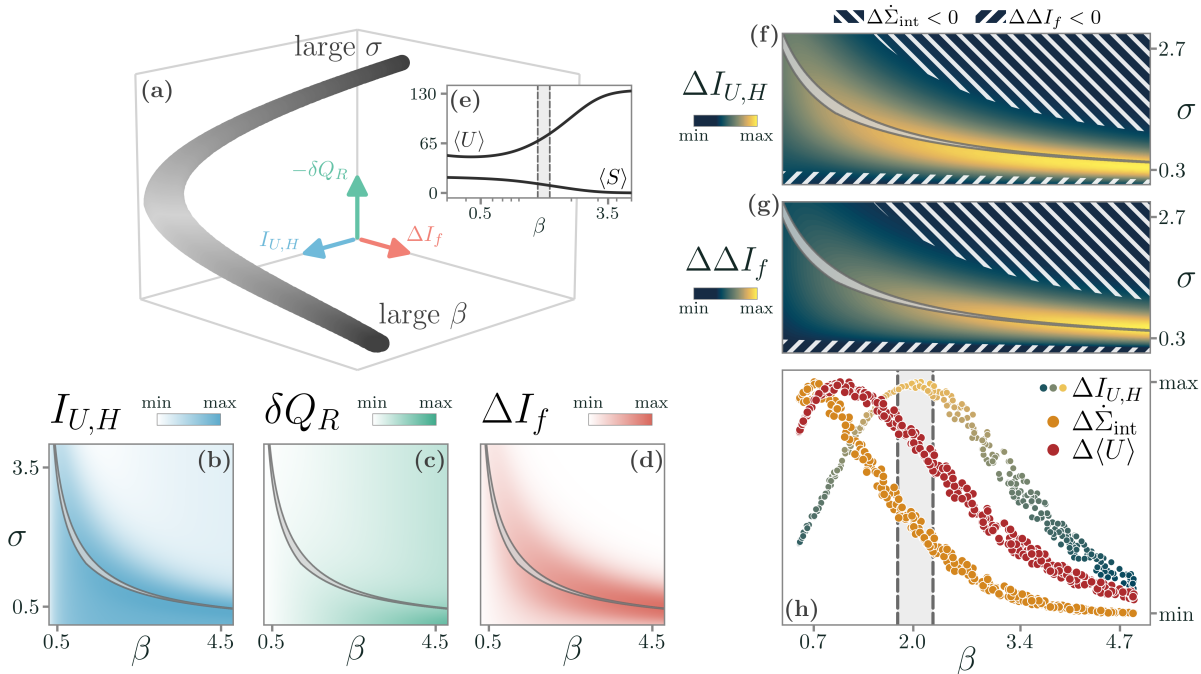


FIG. 3. Trade-off between energy dissipation and information. (a) The optimal surface in the  $(I_{U,H}, \Delta I_f, -\delta Q_R)$  space with a constant external field, obtained through a Pareto-like optimization. (b-d) The values of  $\sigma$  and  $\beta$  inside the optimal surface (gray surface) maximize both the readout information,  $I_{U,H}$ , and the information feedback of the storage population,  $\Delta I_f$ , while minimizing the dissipation of the receptor,  $\delta Q_R$ . (e) At the optimal  $(\beta, \sigma)$  (gray area, shown at a fixed value of  $\sigma \approx 1.5$ ) the average readout,  $\langle U \rangle$ , and storage,  $\langle S \rangle$ , are at intermediate values. (f-g) In the presence of a repeated field, the increase in readout information,  $\Delta I_{U,H}$ , and information feedback,  $\Delta \Delta I_f$ , due to adaptation are both maximal around the optimal values of  $(\beta, \sigma)$  computed at stationarity (gray surface). White stripes indicate regions where adaptation leads to either an increase of entropy production of the internal processes,  $\dot{\Sigma}_{int}$ , or a decrease of  $\Delta \Delta I_f$ . Remarkably, in these regions the system is not acquiring information, as  $\Delta I_{U,H}$  is close to zero. (h) Comparison of the information increase with the reduction in entropy production,  $\Delta \dot{\Sigma}_{int}$ , and the adaptation of the readout,  $\Delta \langle U \rangle$ . Around the static optimal values (gray area, shown at a fixed value of  $\sigma \approx 1.5$ ) adaptation leads to maximal information increase, where both  $\Delta \dot{\Sigma}_{int}$  and  $\Delta \langle U \rangle$  display intermediate values. Model parameters are specified in the Methods.

information,  $\Delta I_{U,H}$ , comparing the response to the first signal with the one to a signal at large times - so that the system has reached a time-periodic steady state. The same quantity can be estimated for feedback information,  $\Delta \Delta I_f$ , average readout concentration,  $\Delta \langle U \rangle$ , and dissipation of internal processes,  $\Delta \dot{\Sigma}_{int}$  (see Supplementary Information). Surprisingly, we find that the optimal surface in the space of  $\beta$  and  $\sigma$  lies in the region in which adaptation and feedback efficacies are both maximized (see Figure 3f-g). Therefore, dynamical features of information processing peak where the system is optimally responsive to a static field. We also report the existence of two regions, away from the optimal surface, for which there is no reduction of dissipation during adaptation (top-right corner of Figures 3f-g) or the feedback is not beneficial (lower dashed region of Figures 3f-g).

Furthermore, the maximum of  $\Delta I_{U,H}$  corresponds to intermediate values of adaptation,  $\Delta \langle U \rangle$ , and dissipation reduction,  $\Delta \dot{\Sigma}_{int}$  (Figure 3h). In fact, values of  $\beta$

for which adaptation is too steep, i.e., to the left of the optimal surface in Figure 3h, lead to high dissipation and the system loses sensitivity to the external signal. Analogously, to the right of the optimal surface, we clearly see that no adaptation results in low dissipation but no information gain. Analyses of different signal and pause durations reveal a non-trivial interplay between finite-time memory and the environment dynamics. In particular, the more the system is exposed to the external signal, the more information it will store and use to adapt, up to the optimal encoding defined by the static picture (see Supplementary Information).

The minimal mechanisms of the presented architecture predict a clear dissipation-information trade-off. Non-equilibrium sensing is more effective in low-noise conditions, as the system dissipation is high, whereas, with strong thermal noise, less energy is required at the price of a lower information gain. Optimal adaptation takes place at the Pareto-like surface, tuning the storage cost

to overcome thermal noise.

### Adaptation dynamics in the visual system of zebrafish larvae

At the sensory level, adaptation manifests as a progressive decay in the amplitude of the neuronal responses to repeated or prolonged sensory stimulation, typically measured as a progressive reduction of the stimulus-driven neuronal firing rate [42–44]. While it is generally accepted and reported that inhibitory feedback mechanisms modulate the stimulus weight [45], there are different theories about the actual functional role of adaptation in controlling the information flow, optimal processing, and sensitivity calibration [44]. To test whether our framework could capture the typical adaptation dynamics exhibited by the visual system of a living organism, we studied the response of zebrafish larvae to repeated stimulation. These widely used model organisms show from the early days of life a robust panel of sensory-driven behaviors, useful for linking neural circuits activity and motor outcomes [46]. We thus adopted an experimental paradigm based on volumetric multiphoton imaging [47]. We optically recorded the neuronal activity of  $\approx 55000$  neurons across the whole brain in response to the repeated presentation of visual stimulation with a dark looming dot on a lighter background. In particular, we extract a subpopulation of  $\approx 2400$  neurons with a temporal activity profile that is most correlated with the stimulation protocol (see Methods). Along with a reliable stimulus-evoked activity, the data showed a progressive decrease in response amplitudes, typical of a sensory adaptation process (Figure 4a). A 2-dimensional embedding of the activity profiles obtained via principal component analysis (PCA) clearly captures the adaptation dynamics (explained variance  $\approx 70\%$ ). While the evolution of the evoked neural response is described by the first principal direction, adaptation reflects into the second one (Figure 4c).

To adjust our model architecture to the mesoscopic scale of the visual system of zebrafish larvae, we identify each readout unit with a subpopulation of neurons. Crucially, we assume that neural activations are stochastic with a given probability (see Methods). These choices allow us to investigate the sole effects of the minimal mechanisms included in our framework, neglecting the specific features of local and global neural dynamics. The patterns of the model-generated raster plot are remarkably similar to those of the fluorescence signal (see Figure 4a-b). Moreover, a PCA of these simulated data reveals that, while the evoked neural response is replaced, as expected, by a switching dynamics, adaptation is once more fully captured along the second principal direction, closely resembling the experimental data. Notably, these results are qualitatively robust with respect to changes in the model parameters, as long as the system lives in the optimal Pareto-like region.

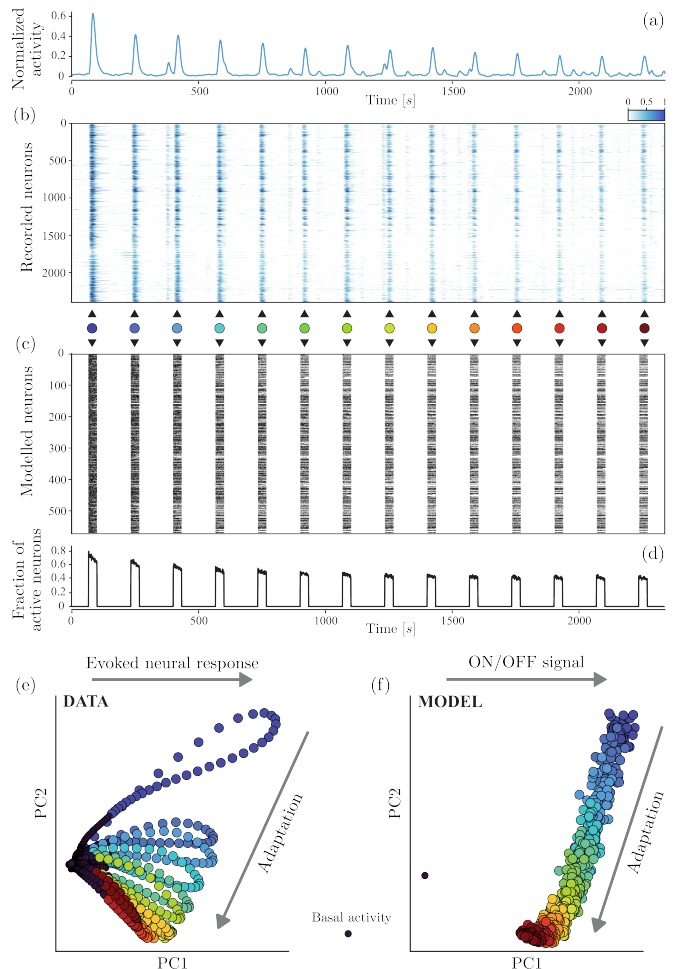


FIG. 4. Adaptation dynamics in zebrafish larvae. (a-b) Normalized neural activity profile in a zebrafish larva in response to the repeated presentation of visual stimulation. Stimuli are indicated with colored dots from blue to red as time increases. (c) Raster plot of firing neurons at each time obtained from our model with stochastic neural activations. (d) Fraction of active neurons as a function of time. (e) PCA of experimental data reveals that adaptation is captured by the first two principal components. Adaptation is highlighted along the second principal direction, while features of the evoked neural response by the first one. Different colors indicate different responses to different stimuli. (f) PCA of simulated neural activations. Although we do not model explicitly the evoked neural response, but rather an on/off switch of the signal, the core features of adaptation are correctly captured along the second principal direction. Model parameters are  $\beta = 3.5$  and  $\sigma = 0.1$ , and as specified in the Methods. Different parameters, provided that the model is close to the optimal region shown in Figure 3, do not qualitatively change the results.

This approach unravels the essential role of the minimal ingredients encoded in our model to explain the emergence of adaptation and its functional advantages. Indeed, we are able to capture the basic features of visual adaptation in zebrafish larvae without explicitly modeling the biological processes underlying neural dynamics.

This suggests that the functional advantages of adaptation are rooted in the interplay between energy dissipation and information gain, although biological details remain crucial in shaping the evoked neural response and implementing these emerging features.

### Summary and outlook

Our minimal architecture may serve as an archetypal and coarse-grained description of adaptation and information storage across biological scales, going from biochemical networks to neural response. It is informed by theoretical and experimental observations of different biological systems, and unravels the core mechanisms at the heart of adaptive behaviors. Starting from a chemical description of internal processes, we have characterized how these mechanisms allow the system to encode and store environmental stimuli, creating an effective chemical memory. The resulting information dynamics shows a two-fold advantage of adaptation: reducing the dissipation of internal processes and simultaneously enhancing information processing capabilities. Furthermore, depending on the strength of thermal noise and the cost of storing information, optimal sensing takes place at the edge of an information-dissipation trade-off. Low-noise conditions require higher dissipation but favor information gain.

Crucially, the resulting description, while chemically consistent, can be declined for more coarse-grained systems, where receptors, adaptation, and storage may occur at mesoscopic or macroscopic scales. As a proof of concept, we have employed it to describe sensory adaptation in the neural activity of a zebrafish larva exposed to repeated visual stimuli. Adaptive response is consistently captured without the need for biological details, hinting at the fact that dissipation, negative feedback, and information storage are minimal and necessary building blocks to describe any sensing mechanism. In particular, although here we studied sensory adaptation, it is reasonable to think that motor and, in general, behavioral adaptation [44] may stem from similar physical principles. Future works might unravel these aspects.

Extensions of these ideas are manifold. Although in the present work we focused on adaptation to repetitions of statistically identical signals, it will be interesting to characterize the system's response to diverse environments [48]. To this end, incorporating multiple receptors and/or storage populations may be needed to harvest information in complex conditions. In such scenarios, correlations between external signals may help reduce the encoding effort. On a general ground, understanding how this encoded information is exploited by living systems is far more challenging and fascinating. For example, navigation in spatial environments, both in biological [49, 50] and bio-inspired artificial systems [51, 52], is an emergent behavior governed by how information about surroundings guides decision-making. Moreover, living systems do not passively read and adapt

to external signals, but often act upon the environment. Adaptation dynamics and memory will remain core ingredients to model and grasp the complex information dynamics arising from this feedback mechanism. Further, understanding how information is used at the level of single agents will pave the way for the understanding of how collective intelligence emerges from the interaction of many information-processing units.

Our work serves as a fundamental framework for these ideas. Its main advantage is to provide a molecular description of the necessary mechanisms to support information processing in a wide range of temporal and spatial scales, at the same time being minimal enough to allow for analytical treatments. As a consequence, we believe it may help the experimental quest for signatures of these physical ingredients in a variety of systems, many of which are only described at a phenomenological level. Ultimately, our results show how adaptation - a ubiquitous phenomenon that takes place at strikingly different biological scales - comes along with a thermodynamic and information-based advantage, explaining its relevance for biological systems.

### ACKNOWLEDGMENTS

G.N., S.S., and D.M.B. acknowledge Amos Maritan for fruitful discussions. D.M.B. thanks Paolo De Los Rios for insightful comments. G.N. and D.M.B. acknowledge the Max Planck Institute for the Physics of Complex Systems for hosting G.N. during the initial stage of this work.

## Methods

**Model parameters.** The system is driven out of equilibrium by both the external field and the storage inhibition through the receptor dynamics, whose dissipation per unit temperature is  $\delta Q_R$  (see Eq. (6)). The ratio  $g = \Gamma_H^0/\Gamma_I^0$  sets the relative timescales of the two receptor pathways (see Eq. (1)). The energetic barrier ( $V - cr$ ) fixes the average values of the readout population both in the passive and active state, namely  $\langle U \rangle_P = e^{-\beta V}$  and  $\langle U \rangle_A = e^{-\beta(V-c)}$  (see Eq. (2)), and  $\kappa$  controls the effectiveness of the storage in inhibiting the receptor's activation. We assume that, on average, the activation rate due to the field is balanced by the feedback of a fraction  $\alpha = \langle S \rangle / N_S$  of the storage population,

$$\left\langle \log \frac{\Gamma_{P \rightarrow A}^{(H)}}{\Gamma_{A \rightarrow P}^{(I)}} \right\rangle = \beta g (\langle H \rangle - \kappa \sigma \alpha) = 0 \quad \rightarrow \quad \kappa = \frac{\langle H \rangle}{\sigma \alpha},$$

so that we only need to fix  $\alpha$ . If not otherwise specified, we set  $g = 1$ , i.e.,  $\Gamma_H^0 = \Gamma_I^0 \equiv \Gamma_R^0$ ,  $\Delta E = 1$ ,  $\langle U \rangle_A = 150$ ,  $\langle U \rangle_P = 0.5$ , and  $\alpha = 2/3$ . We remark that the emerging features of the model are independent of the specific choice of these parameters. Furthermore, we typically consider the average of the exponentially distributed signal to be  $\langle H \rangle_{\max} = 10$  and  $\langle H \rangle_{\min} = 0.1$  (see Supplementary Information).

Overall, we are left with  $\beta$  and  $\sigma$  as free parameters.  $\beta$  quantifies the amount of thermal noise in the system, and at small  $\beta$  the thermal activation of the receptor hinders the effect of the field and makes the system almost unable to process information. Conversely, if  $\beta$  is high, the system must overcome large thermal inertia, increasing the dissipative cost. In this regime of weak thermal noise, we expect that, given a sufficient amount of energy, the system can effectively process information.

**Timescale separation and model solution.** We solve our system in a timescale separation framework [53, 54], where the storage evolve on a timescale which is much slower than all the other internal ones, i.e.,

$$\Gamma_S^0 \ll \Gamma_I^0 \approx \Gamma_H^0 \ll \Gamma_U^0.$$

The fact that  $\Gamma_S^0$  is the slowest timescale at play is crucial to make these components act as an information reser-

voir. This assumption is also compatible with biological examples. The main difficulty arises from the presence of the feedback, i.e. the field influences the receptor and thus the readout population, which in turn impacts the storage population and finally changes the chemical rate of the receptor - schematically,  $H \rightarrow R \rightarrow U \rightarrow S \rightarrow R$ . In order to solve the system, we need to properly take into account these effects.

We start with the master equation for the propagator  $P(u, r, s, h, t|u_0, r_0, s_0, h_0, t_0)$ ,

$$\partial_t P = \left[ \frac{\hat{W}_U(r)}{\tau_U} + \frac{\hat{W}_R(s, h)}{\tau_R} + \frac{\hat{W}_S(u)}{\tau_S} + \frac{\hat{W}_H}{\tau_H} \right] P,$$

where  $\tau_U \ll \tau_R \ll \tau_S \sim \tau_H$  are the timescales of the different processes, e.g.,  $\tau_U = 1/\Gamma_U^0$ . We rescale the time by  $\tau_S$  and introduce two small parameters to control the timescale separation analysis,  $\epsilon = \tau_U/\tau_R$  and  $\delta = \tau_R/\tau_H$ . Since  $\tau_S/\tau_H = \mathcal{O}(1)$ , we set it to 1 without loss of generality. We then write  $P = P^{(0)} + \epsilon P^{(1)}$  and expand the master equation to find  $P^{(0)} = p_{U|R}^{\text{st}}(u|r)\Pi$ , with  $\hat{W}_U p_{U|R}^{\text{st}} = 0$ . Similarly,  $\Pi$  obeys

$$\partial_t \Pi = \left[ \delta^{-1} \hat{W}_R(s, h) + \hat{W}_S(u) + \hat{W}_H \right] \Pi.$$

Yet again,  $\Pi = \Pi^{(0)} + \delta \Pi^{(1)}$  allows us to write  $\Pi^{(0)} = p_{R|S,H}^{\text{st}}(r|s, h)F(s, h, t|s_0, h_0, t_0)$  at order  $\mathcal{O}(\delta^{-1})$ , where  $\hat{W}_R p_{R|S,H}^{\text{st}} = 0$ . Expanding first in  $\epsilon$  and then in  $\delta$  sets a hierarchy among timescales. Crucially, due to the feedback present in the system we cannot solve the next order explicitly to find  $F$ . Indeed, after a marginalization over  $r$ , we find  $\partial_t F = \left[ \hat{W}_H + \hat{W}_S(\bar{u}(s, h)) \right] F$ , at order  $\mathcal{O}(1)$ , where  $\bar{u}(s, h) = \sum_{u,r} u p_{U|R}^{\text{st}}(u|r) p_{R|S,H}^{\text{st}}(r|s, h)$ . Hence, the evolution operator for  $F$  depends manifestly on  $s$ , and the equation cannot be self-consistently solved. To tackle the problem, we first discretize time, considering a small interval, i.e.,  $t = t_0 + \Delta t$  with  $\Delta t \ll \tau_U$  and thus  $\bar{u}(s, h) \approx u_0$ . We thus find  $F(s, h, t|s_0, h_0, t_0) = P(s, t|s_0, t_0)P_H(h, t|h_0, t_0)$  in the domain  $t \in [t_0, t_0 + \Delta t]$ , since  $H$  evolves independently from the system (see also Supplementary Information for analytical steps).

Iterating the procedure for multiple time steps, we end up with a recursive equation for the joint probability  $p_{U,R,S,H}(u, r, s, h, t_0 + \Delta t)$ . We are interested in the following marginalization

$$p_{U,S}(u, t + \Delta t) = \sum_{r=0}^1 \int_0^\infty dh p_{U|R}^{\text{st}}(u|r) p_{R|S,H}^{\text{st}}(r|h, s) p_H(h, t + \Delta t) \sum_{s'=0}^{N_S} \sum_{u'=0}^\infty P(s', t \rightarrow s, t + \Delta t|u') p_{U,S}(u', s', t) \quad (\text{M1})$$

where  $P(s', t \rightarrow s, t + \Delta t)$  is the propagator of the storage

at fixed readout. This is the Chapman-Kolmogorov equa-

tion in the time-scale separation approximation. Notice that this solution requires the knowledge of  $p_{U,S}$  at the previous time-step and it has to be solved iteratively.

**Explicit solution for the storage propagator.** To find a numerical solution to our system, we first need to compute the propagator  $P(s_0, t_0 \rightarrow s, t)$ . Formally, we have to solve the master equation

$$\begin{aligned} \partial_t P(s_0 \rightarrow s|u_0) = \Gamma_S^0 \left[ e^{-\beta\sigma} u_0 P(s_0 \rightarrow s') \delta_{s',s-1} + \right. \\ \left. + s' P(s_0 \rightarrow s') \delta_{s',s+1} + \right. \\ \left. - P(s_0 \rightarrow s') \delta_{s',s} (s' + e^{-\beta\sigma} u_0) \right] \end{aligned} \quad (\text{M2})$$

where we used the shorthand notation  $P(s_0 \rightarrow s) = (s_0, t_0 \rightarrow s, t)$ . Since our formula has to be iterated for small time-steps, i.e.,  $t - t_0 = \Delta t \ll 1$ , we can write the propagator as follows

$$P(s_0, t_0 \rightarrow s, t_0 + \Delta t|u_0) = p_{S|U}^{\text{st}} + \sum_{\nu} w_{\nu} a^{(\nu)} e^{\lambda_{\nu} \Delta t} \quad (\text{M3})$$

where  $w_{\nu}$  and  $\lambda_{\nu}$  are respectively eigenvectors and eigenvalues of the transition matrix  $\hat{W}_S(u_0)$ ,

$$\begin{aligned} (\hat{W}_S(u_0))_{ij} &= e^{-\beta\sigma} u_0 & \text{if } i = j + 1 \\ (\hat{W}_S(u_0))_{ij} &= j & \text{if } i = j - 1 \\ (\hat{W}_S(u_0))_{ij} &= 0 & \text{otherwise} \end{aligned} \quad (\text{M4})$$

and the coefficients  $a^{(\nu)}$  are such that

$$p_{S|U}(s_0, t_0 \rightarrow s, t_0 + \Delta t|u_0) = p_{S|U}^{\text{st}} + \sum_{\nu} w_{\nu} a^{(\nu)} = \delta_{s,s_0}. \quad (\text{M5})$$

Since eigenvalues and eigenvectors of  $\hat{W}_S(u_0)$  might be computationally expensive to find, we employ another simplification. As  $\Delta t \rightarrow 0$ , we can restrict the matrix only to jumps to the  $n$ -th nearest neighbors of the initial state  $(s_0, t_0)$ , assuming that all other states are left unchanged in small time intervals.

**Mutual information.** Once we have  $p_U(u, t)$  (obtained marginalizing  $p_{U,S}$  over  $s$ ) for a given  $p_H(h, t)$ , we can compute the mutual information

$$I_{U,H}(t) = \mathcal{S}[p_U](t) - \int_0^{\infty} dh p_H(h, t) \mathcal{S}[p_{U|H}](t)$$

where  $\mathcal{S}$  is the Shannon entropy. For the sake of simplicity, we consider that the external field follows an exponential distribution  $p_H(h, t) = \lambda(t) e^{-\lambda(t)h}$ . Notice that, in order to determine such quantity, we need the conditional probability  $p_{U|H}(u, t)$ . In the Supplementary Information, we show how all the necessary joint and conditional probability distributions can be computed from the dynamical evolution derived above.

We also highlight here that the timescale separation implies  $I_{S,H} = 0$ , since

$$\begin{aligned} p_{S|H}(s, t|h) &= \sum_u p_{U,S|H}(u, s, t|h) \\ &= p_S(s, t) \sum_u \sum_r p_{U|R}^{\text{st}}(u|r) p_{R|S,H}^{\text{st}}(r|s, h) \\ &= p_S(s, t). \end{aligned}$$

Although it may seem surprising, this is a direct consequence of the fact that  $S$  is only influenced by  $H$  through the stationary state of  $U$ . Crucially, the presence of the feedback is still fundamental to promote adaptation. Indeed, we can always write the mutual information between the field  $H$  and both the readout  $U$  and the storage  $S$  together as  $I_{(U,S),H} = \Delta I_f + I_{U,H}$ , where  $\Delta I_f = I_{(U,S),H} - I_{U,H} = I_{(U,H),S} - I_{U,S}$ . Hence, if we have  $\Delta I_f > 0$  (as we shown in the main text), the storage is increasing the information of the two populations together on the external field. Overall, although  $S$  and  $H$  are independent in this limit, the feedback is paramount in shaping how the system responds to the external field and stores information about it.

**Dissipation of internal chemical processes.** The production of readout,  $u$ , and storage,  $s$ , molecules requires energy. The dissipation into the environment can be quantified from the environmental contribution of the Schnakenberg entropy production, which is also the only one that survives at stationarity [55]. We have:

$$\begin{aligned} \dot{\Sigma}_{\text{int}} &= \sum_{u,s} (\Gamma_{u \rightarrow u+1} p_{U,S}(u, s, h, t) + \\ &\quad - \Gamma_{u+1 \rightarrow u} p_{U,S}(u+1, s, h, t)) \log \frac{\Gamma_{u \rightarrow u+1}}{\Gamma_{u+1 \rightarrow u}} + \\ &\quad + \sum_{u,s} (\Gamma_{s \rightarrow s+1} p_{U,S}(u, s, h, t) + \\ &\quad - \Gamma_{s+1 \rightarrow s} p_{U,S}(u, s+1, h, t)) \log \frac{\Gamma_{s \rightarrow s+1}}{\Gamma_{s+1 \rightarrow s}} \end{aligned} \quad (\text{M6})$$

where we indicated all possible dependencies in the joint probability distribution. By employing the timescale separation [53], and noting that  $\Gamma_{u \rightarrow u \pm 1}$  do not depend on  $s$ , we finally have:

$$\begin{aligned} \dot{\Sigma}_{\text{int}} &= \sum_{u,s} (\Gamma_{s \rightarrow s+1} p_{U,S}(u, s, h, t) + \\ &\quad - \Gamma_{s+1 \rightarrow s} p_{U,S}(u, s+1, h, t)) \log \frac{\Gamma_{s \rightarrow s+1}}{\Gamma_{s+1 \rightarrow s}} \end{aligned} \quad (\text{M7})$$

As this quantity decreases during adaptation, the system tends to dissipate less and less into the environment to produce the internal chemical populations that are required to encode and store the external signal.

**Pareto-like optimization.** We first perform a Pareto-like optimization at stationarity in the presence of a large, but static, external field. We seek the optimal values of

$(\beta, \sigma)$  by maximizing the functional

$$\mathcal{L}(\beta, \sigma) = \gamma_1 \frac{I_{U,H}(\beta, \sigma)}{\max(I_{U,H})} + \gamma_2 \frac{\Delta I_f(\beta, \sigma)}{\max(\Delta I_f)} + (1 - \gamma_1 - \gamma_2) \frac{\delta Q_R(\beta, \sigma)}{\max(\delta Q_R)} \quad (\text{M8})$$

where  $\gamma_1 + \gamma_2 \in [0, 1]$ . Hence, we maximize both the information between the readout and the field, and the information feedback, i.e. how much this mechanism enhances encoding information about the signal. Simultaneously, we minimize the dissipation of the receptor induced by both the signal and feedback process. The values are normalized since, in principle, they can span different orders of magnitudes. Later on, we find that the optimality of the information dynamics with a pulsating signal, in terms of adaptation and feedback efficacy, is attained for values of  $\beta$  and  $\sigma$  lying in the vicinity of this static Pareto-like surface.

**Recording of whole brain neuronal activity in zebrafish larvae.** Acquisitions of the zebrafish brain activity were carried out in *Elavl3:H2BGCaMP6s* larvae at 5 days post fertilization raised at  $28^\circ\text{C}$  on a 12 h light/12 h dark cycle according to the approval by the Ethical Committee of the University of Padua (61/2020 dal Maschio). Larvae were embedded in 2 percent agarose gel and their brain activity was recorded using a multiphoton system with a custom 3D volumetric acquisition module. Data were acquired at 30 frames per second covering an effective field of view of about  $450 \times 900\mu\text{m}$  with a resolution of  $512 \times 1024$  pixels. The volumetric module acquires a volume of about  $180 - 200\mu\text{m}$  in thickness encompassing 30 planes separated by about  $7\mu\text{m}$ , at a rate of 1 volume per second, sufficient to track the slow dynamics associated with the fluorescence-based activity reporter *GCaMP6s*. Visual stimulation was presented in the form of a looming stimulus with 150s intervals, centered with the fish eye. See Supplementary Information.

**Data analysis.** The acquired temporal series were first processed using an automatic pipeline, including motion

artifact correction, temporal filtering with a 3s rectangular window, and automatic segmentation. The obtained dataset was manually curated to resolve segmentation errors or to integrate cells not detected automatically. We fit the activity profiles of about 55000 cells with a linear regression model using a set of base functions representing the expected responses to each stimulation event. These base functions have been obtained by convolving the exponentially decaying kernel of the *GCaMP* signal lifetime with square waveforms characterizing the presentation of the corresponding visual stimulus. The resulting score coefficients of the fit were used to extract the cells whose score fell within the top 5% of the distribution, resulting in a population of  $\approx 2400$  neurons whose temporal activity profile correlates most with the stimulation protocol. The resulting fluorescence signals  $F^{(i)}$  were processed by removing a moving baseline to account for baseline drifting and fast oscillatory noise [56]. See Supplementary Information.

**Model for neural activity.** Here, we describe how our framework is modified to mimic neural activity and reconstruct the raster plot in Figure 4. Each readout molecule is interpreted as a population of  $N$  neurons, i.e., a region dedicated to the sensing of a specific input. Storage can be implemented in different ways, such as inhibitory neural populations or synaptic plasticity mechanisms, and we do not seek a detailed biological interpretation. When a readout population is activated at time  $t$ , each of its  $N$  neurons fires with a probability  $p$ . We set  $N = 100$  and  $p = 0.5$ , but changes in their values do not alter the results presented in the main text. In this way, at each time in which a readout unit is active, firing neurons are generally different even if we do not take into account the underlying neural dynamics. Due to adaptation, some of the readout units activated by the first stimulus will not be activated by subsequent stimuli. Although the evoked neural response cannot be captured by this extremely simple model, its archetypal ingredients (dissipation, storage, and feedback) are informative enough to reproduce the low-dimensional adaptation dynamics found in experimental data.

- 
- [1] G. Tkačik and W. Bialek, Information processing in living systems, *Annual Review of Condensed Matter Physics* **7**, 89 (2016).
  - [2] E. U. Azeloglu and R. Iyengar, Signaling networks: information flow, computation, and decision making, *Cold Spring Harbor perspectives in biology* **7**, a005934 (2015).
  - [3] F. S. Gnesotto, F. Mura, J. Gladrow, and C. P. Broedersz, Broken detailed balance and non-equilibrium dynamics in living systems: a review, *Reports on Progress in Physics* **81**, 066601 (2018).
  - [4] I. Nemenman, Information theory and adaptation, *Quantitative biology: from molecular to cellular systems* **4**, 73 (2012).
  - [5] T. Nakajima, Biologically inspired information theory: Adaptation through construction of external reality models by living systems, *Progress in Biophysics and Molecular Biology* **119**, 634 (2015).
  - [6] M. Whiteley, S. P. Diggle, and E. P. Greenberg, Progress in and promise of bacterial quorum sensing research, *Nature* **551**, 313 (2017).
  - [7] T. J. Perkins and P. S. Swain, Strategies for cellular decision-making, *Molecular systems biology* **5**, 326 (2009).
  - [8] D. E. Koshland Jr, A. Goldbeter, and J. B. Stock, Amplification and adaptation in regulatory and sensory systems, *Science* **217**, 220 (1982).
  - [9] Y. Tu, T. S. Shimizu, and H. C. Berg, Modeling the chemotactic response of *escherichia coli* to time-varying stimuli, *Proceedings of the National Academy of Sciences* **105**, 14855 (2008).

- [10] Y. Tu, The nonequilibrium mechanism for ultrasensitivity in a biological switch: Sensing by Maxwell's demons, *Proceedings of the National Academy of Sciences* **105**, 11737 (2008).
- [11] H. Mattingly, K. Kamino, B. Machta, and T. Emonet, *Escherichia coli* chemotaxis is information limited, *Nature Physics* **17**, 1426 (2021).
- [12] R. Cheong, A. Rhee, C. J. Wang, I. Nemenman, and A. Levchenko, Information transduction capacity of noisy biochemical signaling networks, *Science* **334**, 354 (2011).
- [13] H. Wajant, K. Pfizenmaier, and P. Scheurich, Tumor necrosis factor signaling, *Cell Death & Differentiation* **10**, 45 (2003).
- [14] G. Lan, P. Sartori, S. Neumann, V. Sourjik, and Y. Tu, The energy–speed–accuracy trade-off in sensory adaptation, *Nature physics* **8**, 422 (2012).
- [15] A. Menini, Calcium signalling and regulation in olfactory neurons, *Current opinion in neurobiology* **9**, 419 (1999).
- [16] A. Kohn, Visual adaptation: physiology, mechanisms, and functional benefits, *Journal of neurophysiology* **97**, 3155 (2007).
- [17] N. A. Lesica, J. Jin, C. Weng, C.-I. Yeh, D. A. Butts, G. B. Stanley, and J.-M. Alonso, Adaptation to stimulus contrast and correlations during natural visual stimulation, *Neuron* **55**, 479 (2007).
- [18] A. Benucci, A. B. Saleem, and M. Carandini, Adaptation maintains population homeostasis in primary visual cortex, *Nature neuroscience* **16**, 724 (2013).
- [19] E. Schneidman, M. J. Berry, R. Segev, and W. Bialek, Weak pairwise correlations imply strongly correlated network states in a neural population, *Nature* **440**, 1007 (2006).
- [20] G. Tkacik, O. Marre, D. Amodè, E. Schneidman, W. Bialek, and M. J. Berry, Searching for collective behavior in a large network of sensory neurons, *PLoS computational biology* **10**, e1003408 (2014).
- [21] Z. D. Kurtz, C. L. Müller, E. R. Miraldi, D. R. Littman, M. J. Blaser, and R. A. Bonneau, Sparse and compositionally robust inference of microbial ecological networks, *PLoS computational biology* **11**, e1004226 (2015).
- [22] K. Tunström, Y. Katz, C. C. Ioannou, C. Huepe, M. J. Lutz, and I. D. Couzin, Collective states, multistability and transitional behavior in schooling fish, *PLoS computational biology* **9**, e1002915 (2013).
- [23] G. Nicoletti and D. M. Busiello, Mutual information disentangles interactions from changing environments, *Physical Review Letters* **127**, 228301 (2021).
- [24] G. Nicoletti and D. M. Busiello, Mutual information in changing environments: non-linear interactions, out-of-equilibrium systems, and continuously-varying diffusivities, *Physical Review E* **106**, 014153 (2022).
- [25] R. De Smet and K. Marchal, Advantages and limitations of current network inference methods, *Nature Reviews Microbiology* **8**, 717 (2010).
- [26] G. Nicoletti, A. Maritan, and D. M. Busiello, Information-driven transitions in projections of underdamped dynamics, *Physical Review E* **106**, 014118 (2022).
- [27] A. Celani, T. S. Shimizu, and M. Vergassola, Molecular and functional aspects of bacterial chemotaxis, *Journal of Statistical Physics* **144**, 219 (2011).
- [28] M. Kollmann, L. Løvdok, K. Bartholomé, J. Timmer, and V. Sourjik, Design principles of a bacterial signalling network, *Nature* **438**, 504 (2005).
- [29] W. H. de Ronde, F. Tostevin, and P. R. Ten Wolde, Effect of feedback on the fidelity of information transmission of time-varying signals, *Physical Review E* **82**, 031914 (2010).
- [30] J. Selimkhanov, B. Taylor, J. Yao, A. Pilko, J. Albeck, A. Hoffmann, L. Tsimring, and R. Wollman, Accurate information transmission through dynamic biochemical signaling networks, *Science* **346**, 1370 (2014).
- [31] N. Barkai and S. Leibler, Robustness in simple biochemical networks, *Nature* **387**, 913 (1997).
- [32] J. M. Parrondo, J. M. Horowitz, and T. Sagawa, Thermodynamics of information, *Nature physics* **11**, 131 (2015).
- [33] C. H. Bennett, The thermodynamics of computation — a review, *International Journal of Theoretical Physics* **21**, 905 (1982).
- [34] T. Sagawa and M. Ueda, Minimal energy cost for thermodynamic information processing: measurement and information erasure, *Physical review letters* **102**, 250602 (2009).
- [35] D. Hartich, A. C. Barato, and U. Seifert, Nonequilibrium sensing and its analogy to kinetic proofreading, *New Journal of Physics* **17**, 055026 (2015).
- [36] M. Skoge, S. Naqvi, Y. Meir, and N. S. Wingreen, Chemical sensing by nonequilibrium cooperative receptors, *Physical review letters* **110**, 248102 (2013).
- [37] I. Lestas, G. Vinnicombe, and J. Paulsson, Fundamental limits on the suppression of molecular fluctuations, *Nature* **467**, 174 (2010).
- [38] S. J. Coultrap and K. U. Bayer, Camkii regulation in information processing and storage, *Trends in neurosciences* **35**, 607 (2012).
- [39] P. W. Frankland and S. A. Josselyn, In search of the memory molecule, *Nature* **535**, 41 (2016).
- [40] J. Lisman, H. Schulman, and H. Cline, The molecular basis of camkii function in synaptic and behavioural memory, *Nature Reviews Neuroscience* **3**, 175 (2002).
- [41] V. Ngampruetikorn, D. J. Schwab, and G. J. Stephens, Energy consumption and cooperation for optimal sensing, *Nature communications* **11**, 1 (2020).
- [42] M. S. Malmierca, M. V. Sanchez-Vives, C. Escera, and A. Bendixen, Neuronal adaptation, novelty detection and regularity encoding in audition, *Frontiers in Systems Neuroscience* **8**, 10.3389/fnsys.2014.00111 (2014).
- [43] W. L. Shew, W. P. Clawson, J. Pobst, Y. Karimipناه, N. C. Wright, and R. Wessel, Adaptation to sensory input tunes visual cortex to criticality, *Nature Physics* **11**, 659 (2015).
- [44] J. Benda, Neural adaptation, *Current Biology* **31**, R110 (2021).
- [45] L.-A. Lamiré, M. Haesemeyer, F. Engert, M. Granato, and O. Randler, Inhibition drives habituation of a larval zebrafish visual response, *bioRxiv*, 2022 (2022).
- [46] M. Dal Maschio, J. C. Donovan, T. O. Helmbrecht, and H. Baier, Linking neurons to network function and behavior by two-photon holographic optogenetics and volumetric imaging, *Neuron* **94**, 774 (2017).
- [47] M. Bruzzone, E. Chiarello, M. Albanesi, M. E. Miletto Petrazzini, A. Megighian, C. Lodovichi, and M. Dal Maschio, Whole brain functional recordings at cellular resolution in zebrafish larvae with 3d scanning multiphoton microscopy, *Scientific reports* **11**, 11048 (2021).
- [48] J. Hidalgo, J. Grilli, S. Suweis, M. A. Muñoz, J. R. Banavar, and A. Maritan, Information-based fitness and the

- emergence of criticality in living systems, *Proceedings of the National Academy of Sciences* **111**, 10095 (2014).
- [49] Y. Tu, Quantitative modeling of bacterial chemotaxis: signal amplification and accurate adaptation, *Annual review of biophysics* **42**, 337 (2013).
- [50] F. Carrara, A. Sengupta, L. Behrendt, A. Vardi, and R. Stocker, Bistability in oxidative stress response determines the migration behavior of phytoplankton in turbulence, *Proceedings of the National Academy of Sciences* **118**, e2005944118 (2021).
- [51] B. Liebchen and H. Löwen, Synthetic chemotaxis and collective behavior in active matter, *Accounts of chemical research* **51**, 2982 (2018).
- [52] M. C. Marchetti, J.-F. Joanny, S. Ramaswamy, T. B. Liverpool, J. Prost, M. Rao, and R. A. Simha, Hydrodynamics of soft active matter, *Reviews of modern physics* **85**, 1143 (2013).
- [53] D. M. Busiello, D. Gupta, and A. Maritan, Coarse-grained entropy production with multiple reservoirs: Unraveling the role of time scales and detailed balance in biology-inspired systems, *Physical Review Research* **2**, 043257 (2020).
- [54] S. Bo and A. Celani, Multiple-scale stochastic processes: decimation, averaging and beyond, *Physics reports* **670**, 1 (2017).
- [55] J. Schnakenberg, Network theory of microscopic and macroscopic behavior of master equation systems, *Reviews of Modern physics* **48**, 571 (1976).
- [56] H. Jia, N. L. Rochefort, X. Chen, and A. Konnerth, In vivo two-photon imaging of sensory-evoked dendritic calcium signals in cortical neurons, *Nature protocols* **6**, 28 (2011).

# Supplementary Information: The architecture of information processing in biological systems

## SI. DETAILED SOLUTION OF THE MASTER EQUATION

Consider the transition rates introduced in the main text:

$$\begin{aligned} \Gamma_{P \rightarrow A}^{(H)} &= e^{\beta(h-\Delta E)} \Gamma_H^0 & \Gamma_{A \rightarrow P}^{(H)} &= \Gamma_H^0 \\ \Gamma_{P \rightarrow A}^{(I)} &= e^{-\beta \Delta E} \Gamma_I^0 & \Gamma_{A \rightarrow P}^{(I)} &= \Gamma_I^0 e^{\beta \kappa s / N_s} \\ \Gamma_{u \rightarrow u+1} &= e^{-\beta(V-cr)} \Gamma_U^0 & \Gamma_{u+1 \rightarrow u} &= (u+1) \Gamma_U^0 \\ \Gamma_{s \rightarrow s+1} &= e^{-\beta \sigma} u \Gamma_S^0 & \Gamma_{s+1 \rightarrow s} &= (s+1) \Gamma_S^0. \end{aligned}$$

We set a reflective boundary for the storage at  $s = N_S$ , corresponding to the maximum amount of storage molecules in the system. Moreover, for the sake of simplicity, we take  $\Gamma_I^0 = \Gamma_H^0 \equiv \Gamma_R^0$ . Retracing the steps of the Methods, the Master Equation governing the evolution of the propagator of all variables,  $P(u, r, s, h, t | u_0, r_0, s_0, h_0, t_0)$ , is:

$$\partial_t P = \left[ \frac{\hat{W}_U(r)}{\tau_U} + \frac{\hat{W}_R(s, h)}{\tau_R} + \frac{\hat{W}_S(u)}{\tau_S} + \frac{\hat{W}_H}{\tau_H} \right] P. \quad (\text{S1})$$

We solve this equation employing a timescale separation, i.e.,  $\tau_U \ll \tau_R \ll \tau_S \sim \tau_H$ , where  $\tau_X = \Gamma_X^0$  for  $X = U, R, S$  and  $\tau_H$  is the typical timescale of the signal dynamics. Motivated by several biological examples, we assumed that the readout population undergoes the fastest dynamics, while storage and signal evolution are the slowest ones. Defining  $\epsilon = \tau_U / \tau_R$  and  $\delta = \tau_R / \tau_H$ , and setting  $\tau_S / \tau_H = 1$  without loss of generality, we have:

$$\partial_t P = \left[ \epsilon^{-1} \delta^{-1} \hat{W}_U(r) + \delta^{-1} \hat{W}_R(s, h) + \hat{W}_S(u) + \frac{\tau_S}{\tau_H} \hat{W}_H \right] P. \quad (\text{S2})$$

We propose a solution in the following form,  $P = P^{(0)} + \epsilon P^{(1)}$ . By inserting this expression in the equation above, and solving order by order in  $\epsilon$ , at order  $\epsilon^{-1}$ , we have that:

$$P^{(0)} = p_{U|R}^{\text{st}}(u|r) \Pi(r, h, t | r_0, h_0, t_0) \quad (\text{S3})$$

where  $p^{\text{st}}$  solves the master equation for the readout evolution at a fixed  $r$ :

$$0 = p_{U|R}^{\text{st}}(u+1)[u+1] + p_{U|R}^{\text{st}} \alpha(r) - p_{U|R}^{\text{st}}(u)[u + \alpha(r)] \quad (\text{S4})$$

with  $\alpha(r) = e^{-\beta(V-cr)}$ . Hence,

$$p_{U|R}^{\text{st}}(u|r) = e^{-\alpha(r)} \frac{\alpha(r)^u}{u!}. \quad (\text{S5})$$

At order  $\epsilon^0$ , we find the equation for  $\Pi$ , also reported in the Methods:

$$\partial_t \Pi(r, h, t | r_0, h_0, t_0) = \left[ \delta^{-1} \hat{W}_R(h) + \hat{W}_S(u) + \hat{W}_H \right] \Pi(r, h, t | r_0, h_0, t_0). \quad (\text{S6})$$

To solve this equation, we propose a solution of the form  $\Pi = \Pi^{(0)} + \delta \Pi^{(1)}$ . Hence, again, at order  $\delta^{-1}$ , we have that  $\Pi^{(0)} = p_{R|S,H}^{\text{st}}(r|s, h) F(s, h, t | s_0, h_0, t_0)$ , where  $p_{R|S,H}^{\text{st}}$  satisfy the steady-state equation for the fastest degree of freedom, with all the others fixed. In the case, it is just the solution of the rate equation for the receptor:

$$p_{R|H,S}^{\text{st}}(r=1) = \frac{\Gamma_{P \rightarrow A}^{\text{eff}}}{\Gamma_{P \rightarrow A}^{\text{eff}} + \Gamma_{A \rightarrow P}^{\text{eff}}}, \quad p_{R|H}^{\text{st}}(r=0) = 1 - p_{R|H}^{\text{st}}(r=1, t) \quad (\text{S7})$$

where  $\Gamma_{P \rightarrow A}^{\text{eff}} = \Gamma_{P \rightarrow A}^{(I)} + \Gamma_{P \rightarrow A}^{(H)}$ , and the same for the reverse reaction. At order  $\delta^{-1}$ , we have an equation for  $F$ :

$$\partial_t F(s, h, t | s_0, h_0, t_0) = \sum_{r,u} p_{U|R}^{\text{st}}(u|r) \left[ \hat{W}_S(u) + \hat{W}_H \right] \left[ p_{R|S,H}^{\text{st}}(r|s, h) F(s, h, t | s_0, h_0, t_0) \right] \quad (\text{S8})$$

As already explained in the Methods, due to the feedback, this equation cannot be solved explicitly. Indeed, the operator governing the evolution of  $F$  is:

$$\hat{W}_{\text{eff}} = \hat{W}_H + \sum_u p_{U|S,H}^{\text{st}}(u|s, h) \hat{W}_S(u) = \hat{W}_H + \hat{W}_S \left( \sum_u u p_{U|S,H}^{\text{st}}(u|s, h) \right) = \hat{W}_H + \hat{W}_S(\bar{u}(s, h)) \quad (\text{S9})$$

with  $p_{U|S,H}^{\text{st}}(u|s, h) = \sum_r p_{U|R}^{\text{st}}(u|r) p_{R|S,H}^{\text{st}}(r|s, h)$  and using the linearity of  $\hat{W}_S(u)$ . In order to solve this equation, we shall assume that  $\bar{u}(s, h) = u_0$ , bearing in mind that this approximation holds if  $t$  is small enough, i.e.,  $t = t_0 + \Delta t$  with  $\Delta t \ll \tau_U$ . Therefore, for a small interval, we have:

$$\partial_t F(s, h, t_0 + \Delta t | s_0, h_0, t_0) = \left[ \hat{W}_S(u_0) + \hat{W}_H \right] F(s, h, t | s_0, h_0, t_0) \quad (\text{S10})$$

Overall, we end up with the following joint probability of the model at time  $t_0 + \Delta t$ :

$$\begin{aligned} p_{U,R,S,H}(u, r, s, h, t_0 + \Delta t) &= \\ &= \sum_{u_0, s_0} p_{U|R}^{\text{st}}(u|r) p_{R|S,H}^{\text{st}}(r|s, h) P(s, t_0 + \Delta t | s_0, u_0, t_0) \int dh_0 P_H(h, t_0 + \Delta t | h_0, t_0) p_{U,S,H}(u_0, s_0, h_0, t_0) \\ &= \sum_{u_0, s_0} p_{U|R}^{\text{st}}(u|r) p_{R|S,H}^{\text{st}}(r|s, h) P(s, t_0 + \Delta t | s_0, u_0, t_0) p_{U,S}(u_0, s_0, t_0) p_H(h, t_0 + \Delta t) \end{aligned} \quad (\text{S11})$$

where  $\int dh_0 P_H(h, t_0 + \Delta t | h_0, t_0) p_{U,S,H}(u_0, s_0, h_0, t_0) = p_{U,S}(u_0, s_0, t_0) p_H(h, t_0 + \Delta t)$  since  $H$  at time  $t_0 + \Delta t$  is independent of  $S$  and  $U$ . When propagating the evolution through intervals of duration  $\Delta t$ , we also assume that  $H$  evolves independently since it is an external variable, while affecting the evolution of the other degrees of freedom. This structure reflects into the equation above. For simplicity, we prescribe  $p_H(h, t)$  to be an exponential distribution,  $p_H(h, t) = \lambda(t) e^{-\lambda(t)h}$ , and solve iteratively Eq. (S11) from  $t_0$  to a given  $T$  in steps of duration  $\Delta t$ , as indicated above. This complex iterative solution arises from the timescale separation because of the cyclic feedback structure:  $\{S, H\} \rightarrow R \rightarrow U \rightarrow S$ . This solution corresponds explicitly to

$$p_{U,S}(u, t + \Delta t) = \sum_{r=0}^1 \int_0^\infty dh p_{U|R}^{\text{st}}(u|r) p_{R|S,H}^{\text{st}}(r|h, s) p_H(h, t + \Delta t) \sum_{s'=0}^{N_S} \sum_{u'=0}^\infty P(s', t \rightarrow s, t + \Delta t | u') p_{U,S}(u', s', t) \quad (\text{S12})$$

where  $P(s', t \rightarrow s, t + \Delta t)$  is the propagator of the storage at fixed readout. This is the Chapman-Kolmogorov equation in the time-scale separation approximation. Notice that this solution requires the knowledge of  $p_{U,S}$  at the previous time-step and it has to be solved iteratively. Both  $p_U$  and  $p_S$  can be obtained by an immediate marginalization.

As detailed in the Methods, the propagator  $P(s_0, t_0 \rightarrow s, t)$ , when restricted to small time intervals, can be obtained by solving the birth-and-death process for storage molecules at fixed readout restricting the state space only to  $n$  nearest neighbors (we checked that our results are robust increasing  $n$  for the selected simulation time step).

### SIII. INFORMATION-THEORETIC QUANTITIES

By direct marginalization of Eq. (S12), we obtain the evolution of  $p_U(u, t)$  and  $p_S(s, t)$  for a given  $p_H(h, t)$ . Hence, we can compute the mutual information as follows:

$$I_{U,H}(t) = \mathcal{H}_U(t) - \int_0^\infty dh p_H(h, t) \mathcal{H}_{U|H}(t) = -\frac{\Delta \mathbb{S}_U}{k_B} \quad (\text{S13})$$

where  $\mathcal{H}_X$  is the Shannon entropy of  $X$ , and  $\Delta \mathbb{S}_U$  is the reduction in the entropy of  $U$  due to repeated measurement (see main text). Notice that, in order to determine such quantity, we need the conditional probability  $p_{U|H}(u, t)$ . This distribution represent the probability that, at a given time, the system jumps at a value  $u$  in the presence of a given field  $h$ . In order to compute it, we can write

$$p_{U|H}(u, t + \Delta t) = \sum_{s=0}^{M_S} \sum_{r=0}^1 p_{U|R}^{\text{st}}(u|r) p_{R|S,H}^{\text{st}}(r|h, s) p_S(s, t + \Delta t) \quad (\text{S14})$$

by definition. The only dependence on  $h$  enters in  $p_{R|S,H}^{\text{st}}$  through the  $e^{\beta h}$  dependence in the rates.

Analogously, all the other mutual information can be obtained. Notably, as we showed in the Methods,  $I_{S,H} = 0$ , as a consequence of the time-scale separation. Crucially, the presence of the feedback is still fundamental to effectively process information about the signal. In particular, let us define  $\Delta I_f = I_{(U,S),H} - I_{U,H}$  as the feedback information, as it quantifies the information how much the knowledge of  $S$  and  $U$  together helps encoding information about the signal with respect to  $U$  alone. We find  $\Delta I_f > 0$ , indicating a positive effect of the feedback during adaptation. In other terms, from Eq. (S13), we have:

$$k_B \Delta I_f = -\Delta \mathbb{S}_{U,S} + \Delta \mathbb{S}_U > 0 \quad (\text{S15})$$

highlighting how much the effect of  $S$  (feedback) reduces the entropy of the system due to repeated measurements.

Practically speaking, in order to evaluate  $I_{(U,S),H}$ , we exploit the following equality:

$$I_{(U,S),H} = \mathcal{S}[p_{U,S}] (t) - \int_0^\infty dh p_H(h,t) \mathcal{S}[p_{U,S|H}] (t). \quad (\text{S16})$$

for which we need  $p_{U,S|H}$ , that can be found noting that

$$p_{U,S}(u, s, t) = p_{U|S}(u, t|s) p_S(s, t) = \int dh \sum_r p_{U|R}^{\text{st}}(u|r) p_{R|S,H}^{\text{st}}(r|s, h) p_S(s, t) p_H(h, t) \quad (\text{S17})$$

from which we immediately see that

$$p_{U,S|H}(u, s, t) = \sum_{r=0}^1 p_{U|R}^{\text{st}}(u|r) p_{R|S,H}^{\text{st}}(r|h, s) p_S(s, t) \quad (\text{S18})$$

which we can easily computed at any given time  $t$ .

### SIII. MEAN-FIELD RELATION BETWEEN AVERAGE READOUT AND STORAGE

Fixing all model parameters, the average value of storage,  $\langle S \rangle$ , and readout,  $\langle U \rangle$ , is numerically determined by solving iteratively the system, as shown above. However, an analytical relation between these two quantities can be found starting from the definition of  $\langle U \rangle$ :

$$\langle U \rangle = \sum_{u,s} u P_{U,S}^{\text{st}}(u, s) = \sum_{u,s} u P_{U|S}^{\text{st}}(u|s) P_S^{\text{st}}(s) = \sum_{u,s,r} u P_{U|R}^{\text{st}}(u|r) P_{R|S}^{\text{st}}(r|s) P_S^{\text{st}}(s) \quad (\text{S19})$$

Then, inserting the expression for the stationary probability that we know analytically:

$$\langle U \rangle = \sum_s \left( \langle u P_{U|R}^{\text{st}}(u|r=0) \rangle P_{R|S}^{\text{st}}(r=0|s) + \langle u P_{U|R}^{\text{st}}(u|r=1) \rangle P_{R|S}^{\text{st}}(r=1|s) \right) P_S^{\text{st}}(s) \quad (\text{S20})$$

where  $P_{R|S}^{\text{st}} = \int dh P_{R|H,S}^{\text{st}} P_H dh \equiv f_R(\rho_S)$  has a complicated expression involving the hypergeometric function  ${}_2F_1$  in terms of model parameters and only the concentration of  $S$ ,  $\rho_S = s/N_S$  (the explicit derivation of this formula is not shown here). Then, we have:

$$\langle U \rangle = \sum_s \left( e^{-\beta V} f_0(\rho_S) + e^{-\beta(V-c)} (1 - f_0(\rho_S)) \right) P_S^{\text{st}}(s) \quad (\text{S21})$$

Since we do not have an analytical expression for  $P_S^{\text{st}}(s)$ , we employ the mean-field approximation, reducing all the correlation functions to products of averages:

$$\langle U \rangle = e^{-\beta(V-c)} + e^{-\beta V} f_0(\bar{\rho}_S) (1 - e^{\beta c}) \quad (\text{S22})$$

where  $\bar{\rho}_S = \langle S \rangle / N_S$ . This clearly shows that, given a set of model parameters,  $\langle U \rangle$  and the average concentration of storage,  $\bar{\rho}_S$  are related. In particular, introducing the change of parameters presented in the Methods, we have the following collapse:

$$\frac{\langle U \rangle - \langle U \rangle_A}{\langle U \rangle_A - \langle U \rangle_P} = f_0(\bar{\rho}_S) \quad (\text{S23})$$

It is also possible to perform an expansion of  $f_0$  which numerically results to be very precise:

$$\frac{\langle U \rangle - \langle U \rangle_A}{\langle U \rangle_A - \langle U \rangle_P} = \frac{a_{-1}(\lambda_H, \beta, g)}{z} + a_0(\lambda_H, \beta) + a_1(\lambda_H, \beta, g)z^{-1-\lambda_H/\beta} + a_2(\lambda_H, \beta)z^{-\lambda_H/\beta} \quad (\text{S24})$$

where  $z = e^{\beta\Delta E} (1 + g e^{\beta\bar{\rho}_S/\alpha\lambda_H})$ . Since all these relations just depend on the average concentration of the storage, it is natural to ask what happens when  $N_S \rightarrow N'_S = nN_S$ . Fixing all the remaining parameters, both  $\langle U \rangle$  and  $\bar{\rho}_S$  will change, still satisfying the mutual relation presented above. Let us consider, for  $N'_S$ , the stationary solution that has the same concentration of S, i.e.,  $(\bar{\rho}_S)_{N'_S} = (\bar{\rho}_S)_{N_S}$ . As a consequence of the scaling relation,  $\langle U \rangle_{N'_S} \neq \langle U \rangle_{N_S}$ . Considering  $\langle U \rangle_P \approx 0$  in both settings, we can ask ourselves what is the factor  $\gamma$  such that  $\gamma(\langle U \rangle_A)_{N_S} = (\langle U \rangle_A)_{N'_S}$ . Since  $u$  only enters linearly in the dynamics of the storage, and the mutual relation only depends on the concentration of  $S$ , we guess that  $\gamma = 1/n$ , as numerically observed. We can finally conclude that the storage concentration is the most relevant quantity of our model to determine feedback, and to characterize its dynamical evolution. This observation makes our conclusions more robust, as they do not depend on the specific choice for the storage reservoir since there always exists a scaling relation connecting  $\langle U \rangle$  and  $\bar{\rho}_S$ .

### A. Information-theoretic inequalities

Let us start with the following equality:

$$\begin{aligned} I_{(U,S),H} &= \sum_{u,s} \int dh p_{U,S,H} \log \frac{p_{U,S,H}}{p_{U,S}p_H} = \sum_{u,s} \int dh p_{U,S,H} \log \frac{p_{U,S|H}}{p_{U,S}} = \sum_{u,s} \int dh p_{U,S,H} \left[ \log \frac{p_{S|PU}}{p_{U,S}} + \log \frac{p_{U|S,H}}{p_U} \right] = \\ &= \log \frac{p_{U|S,HP}p_{S|PU}}{p_{U,S}p_U} = -I_{U,S} + \sum_{u,s} \int dh p_{U,S,H} \left[ \log \frac{p_{U|S,HPH}}{p_{U,H}} + \log \frac{p_{U,H}}{p_{U,PH}} \right] \\ &= -I_{U,S} + I_{U,H} + \sum_{u,s} \int dh p_{U,S,H} \log \frac{p_{U,H|S}p_S}{p_{U,H}p_S} = -I_{U,S} + I_{U,H} + I_{(U,H),S} \end{aligned} \quad (\text{S25})$$

Naming  $\Delta\mathbb{S}_U \equiv \Delta\mathbb{S}_{\text{encode}}$ , since it is the entropy change due to information encoding, and  $k_B(\mathcal{H}_{S|U} - \mathcal{H}_S) = -k_B I_{U,S} \equiv \Delta\mathbb{S}_{\text{store}}$ , since it is the entropy change only due to the storage, we have:

$$k_B \Delta I_f \geq \Delta\mathbb{S}_{\text{store}} \quad k_B \Delta I_f \geq \Delta\mathbb{S}_{\text{encode}} \quad (\text{S26})$$

where the second one directly comes from the definition in Eq. (S15). These relations unravel that the information that the system gains through the feedback is higher than the entropy change due to encoding and storage only, hinting at the fact that internal chemical processes may enhance information-processing operations.

## SIV. THE NECESSITY OF STORAGE

Let us imagine to have the same system we presented in the main text, without the presence of storage molecules. We will first investigate the possibility that negative feedback, necessary for adaptation, is implemented directly through the readout populations that undergoes a fast dynamics. We will analytically show that this limit leads to the absence of adaptation, hinting at the necessity of having a slow dynamical feedback in the system (Sec. SIV A). Afterwards, we will study the system in the limit in which  $U$  applies the feedback, bypassing the role of  $S$ , and it is also a slow variable. Solving the Master Equation through our iterative numerical method, we show that, also in this case, adaptation disappears (Sec. SIV B). These results suggest that not only the feedback has to be applied by a slow variables, but that such a slow variable must have a role different from the readout population. The model proposed in the main text is indeed minimal in this respect, other than compatible with biological examples.

### A. Dynamical feedback cannot be implemented by a fast readout

If the storage is directly implemented by the readout population, the transition rates gets modified as follows:

$$\begin{aligned} \Gamma_{P \rightarrow A}^{(H)} &= e^{\beta(h-\Delta E)} \Gamma_R^0 & \Gamma_{A \rightarrow P}^{(H)} &= \Gamma_R^0 \\ \Gamma_{P \rightarrow A}^{(C)} &= e^{-\beta\Delta E} \Gamma_R^0 & \Gamma_{A \rightarrow P}^{(C)} &= e^{\beta\theta u} \Gamma_R^0 \\ \Gamma_{u \rightarrow u+1} &= e^{-\beta(V-cr)} \Gamma_U^0 & \Gamma_{u+1 \rightarrow u} &= \Gamma_U^0(u+1) \end{aligned} \quad (\text{S27})$$

At this level,  $\theta$  is a free parameter playing the same role as  $\kappa/N_S$  in the complete model with the storage. We start again from the master equation for the propagator  $P(u, r, h, t|u_0, r_0, h_0, t_0)$ :

$$\partial_t P = \left[ \frac{\hat{W}_U(r)}{\tau_U} + \frac{\hat{W}_R(u, h)}{\tau_R} + \frac{\hat{W}_H}{\tau_H} \right] P, \quad (\text{S28})$$

where  $\tau_U \ll \tau_R \ll \tau_H$ , since we are assuming, as before, that  $U$  is the fastest variable. Here,  $\epsilon = \tau_U/\tau_R$  and  $\delta = \tau_R/\tau_H$ . Notice that now  $\hat{W}_R$  depends also on  $u$ . We can solve the system again resorting to a timescale separation and scaling the time by the slowest timescale,  $\tau_H$ . We have:

$$\partial_t P = \left[ \epsilon^{-1} \delta^{-1} \hat{W}_U(r) + \delta^{-1} \hat{W}_R(u, h) + \hat{W}_H \right] P. \quad (\text{S29})$$

We now expand the propagator at first order in  $\epsilon$ ,  $P = P^{(0)} + \epsilon P^{(1)}$ . Then, the order  $\epsilon^{-1}$  of the master equation gives, as above,  $P^{(0)} = p_{U|R}^{\text{st}}(u|r)\Pi(r, h, t|r_0, h_0, t_0)$ . At order  $\epsilon^0$ , Eq. (S29) leads to

$$\partial_t \Pi(r, h, t|r_0, h_0, t_0) = \left[ \delta^{-1} \sum_u \hat{W}_R(u, h) p_{U|R}^{\text{st}}(u|r) + \hat{W}_H \right] \Pi(r, h, t|r_0, h_0, t_0). \quad (\text{S30})$$

To solve this, we expand the propagator as  $\Pi = \Pi^{(0)} + \delta \Pi^{(1)}$  and, at order  $\delta^{-1}$ , we obtain:

$$\left( \sum_u \hat{W}_R(u, h) p_{U|R}^{\text{st}}(u|r) \right) \Pi^{(0)} = 0 \quad (\text{S31})$$

This is a  $2 \times 2$  effective matrix acting on  $\Pi^{(0)}$ , where the only rate affected by  $u$  is  $\Gamma_{A \rightarrow P}^{(C)}$ , which multiplies the active states, i.e.,  $r = 1$ . This equation can be analytically computed and the solution of Eq. (S31) is:

$$\Pi^{(0)} = \rho_{R|H}^{\text{st}}(r|h) f(h, t|h_0, t_0) \quad \rho_{R|H}^{\text{st}}(r=0|h) = \frac{e^{\beta \Delta E} (1 + \Theta)}{e^{\beta h} + 1 + e^{\beta \Delta E} (1 + \Theta)} \quad (\text{S32})$$

with  $\Theta = e^{\beta(V-c)(e^{\beta\theta}-1)}$ . Clearly,  $\rho_{R|H}^{\text{st}}(r|h)$  does not depend on  $u$  since we summed over the fast variable. Going on with the computation, at order  $\delta^0$ , we obtain:

$$\partial_t f(h, t|h_0, t_0) = \hat{W}_H f(h, t|h_0, t_0) \quad (\text{S33})$$

So that the full propagator results to be:

$$P^{(0)}(u, r, h, t|u_0, r_0, h_0, t_0) = p_{U|R}^{\text{st}}(u|r) \rho_{R|H}^{\text{st}}(r|h) P_H(h, t|h_0, t_0) \quad (\text{S34})$$

From this expression, we can find the joint probability distribution, following the same steps as before:

$$p_{U,R,H}(u, r, h, t) = p_{U|R}^{\text{st}}(u|r) \rho_{R|H}^{\text{st}}(r|h) p_H(h, t) \quad (\text{S35})$$

As expected, since  $U$  relaxes instantaneously, the feedback is instantaneous as well. As a consequence, a net adaptation only affects the stationary distribution that is attained at time  $t$ , without any time-dependent effect, finite-time memory, and the emergence of an information dynamics. In other terms, since the timescale of the feedback population is not comparable to the one of the external field,  $U$  will immediately reaches stationarity with an average that is affected by the feedback, and the model does not exhibit a dynamical adaptive behavior.

## B. Effective dynamical feedback requires an additional population

Since the feedback has to act on a timescale comparable to the one of the external signal, we now assume that it is implemented by  $U$ , which is a slow variable. Formally, we take  $\tau_R \ll \tau_U \sim \tau_H$ . Rescaling the time by the slowest timescale,  $\tau_H$  (works the same for  $\tau_U$ ), we have:

$$\partial_t P = \left[ \frac{\tau_H}{\tau_U} \hat{W}_U(r) + \epsilon^{-1} \hat{W}_R(u, h) + \hat{W}_H \right] P \quad (\text{S36})$$

with  $\epsilon = \tau_R/\tau_H$ . We now expand the propagator at first order in  $\epsilon$ ,  $P = P^{(0)} + \epsilon P^{(1)}$ . Then, the order  $\epsilon^{-1}$  of the master equation is simply  $\hat{W}_R P^{(0)} = 0$ , whose solution gives  $P^{(0)} = p_{R|U,H}^{\text{st}}(r|u, h)\Pi(u, h, t|u_0, h_0, t_0)$ . At order  $\epsilon^0$ :

$$\partial_t \Pi(u, h, t|u_0, h_0, t_0) = \left[ \frac{\tau_H}{\tau_U} \sum_r \hat{W}_U(r) p_{R|U,H}^{\text{st}}(r|u, h) + \hat{W}_H \right] \Pi(u, h, t|u_0, h_0, t_0). \quad (\text{S37})$$

The only dependence on  $r$  in  $\hat{W}_U(r)$  is through the production rate of  $U$ . Indeed, the effective transition matrix governing the birth-and-death process of readout molecules is characterized by:

$$\Gamma_{u \rightarrow u+1}^{\text{eff}} = e^{-\beta V} \left( e^{\beta c} p_{R|U,H}^{\text{st}}(r=1|u, h) + p_{R|U,H}^{\text{st}}(r=0|u, h) \right) \Gamma_U^0 \quad (\text{S38})$$

This rate depends only on  $h$ , but  $h$  evolves in time. Therefore, we should scan all possible (infinite) values that  $h$  takes and build an infinite dimensional transition matrix. In order to solve the system, imagine that we are looking at the interval  $[t_0, t_0 + \Delta t]$ . Then, we can employ the following approximation if  $\Delta t \ll \tau_H$ :

$$\Gamma_{u \rightarrow u+1}^{\text{eff}}(h) = \Gamma_{u \rightarrow u+1}^{\text{eff}}(h_0) \quad (\text{S39})$$

Using this simplification, we need to solve the following equation:

$$\partial_t \Pi(u, h, t_0 + \Delta t|u_0, h_0, t_0) = \left[ \frac{\tau_H}{\tau_U} \hat{W}_U^{\text{eff}}(u, h_0) + \hat{W}_H \right] \Pi(u, h, t_0 + \Delta t|u_0, h_0, t_0). \quad (\text{S40})$$

The explicit solution in the interval  $t \in [t_0, t_0 + \Delta t]$  can be found to be:

$$\Pi(u, h, t_0 + \Delta t|u_0, h_0, t_0) = P_U^{\text{eff}}(u, t_0 + \Delta t|u_0, h_0, t_0) P_H(h, t_0 + \Delta t|h_0, t_0) \quad (\text{S41})$$

with  $P_U^{\text{eff}}$  a propagator. The full propagator at time  $t_0 + \Delta t$  is then:

$$p_{U,R,H}(u, r, h, t_0 + \Delta t|u_0, r_0, h_0, t_0) = \sum_{u_0} p_{R|U,H}^{\text{st}}(r|u, h) P_U^{\text{eff}}(u, t_0 + \Delta t|u_0, h_0, t_0) P_H(h, t_0 + \Delta t|h_0, t_0) p_{U,H}(u_0, h_0, t_0) \quad (\text{S42})$$

Integrating over the initial conditions, we finally obtain:

$$p_{U,R,H}(u, r, h, t_0 + \Delta t) = \sum_{u_0} p_{R|U,H}^{\text{st}}(r|u, h) \int dh_0 P_U^{\text{eff}}(u, t_0 + \Delta t|u_0, h_0, t_0) P_H(h, t_0 + \Delta t|h_0, t_0) p_{U,H}(u_0, h_0, t_0) \quad (\text{S43})$$

Reminding that  $H$  evolves independently from all the other variables, we let it evolve first, assuming that the system feels the signal at  $t_0 + \Delta t$ . Since first we set  $h$  to be equal to  $h_0$ , this approximation is again a reasonable assumption only in the limit  $\Delta t \ll \tau_H$ . We have the following resulting joint distribution:

$$p_{U,R,H}(u, r, h, t_0 + \Delta t) = \sum_{u_0} p_{R|U,H}^{\text{st}}(r|u, h) P_U^{\text{eff}}(u, t_0 + \Delta t|u_0, h_{t_0+\Delta t} = h, t_0) p_{U,H}(u_0, h_{t_0+\Delta t} = h, t_0) \quad (\text{S44})$$

where  $h_{t_0+\Delta t}$  is the signal at the end of the time interval. Since  $p_{U,H} = p_{U|H} p_H$ , but  $p_{U|H}$  cannot depend on  $H$  at later times, we have:

$$p_{U,R,H}(u, r, h, t_0 + \Delta t) = \sum_{u_0} p_{R|U,H}^{\text{st}}(r|u, h) P_U^{\text{eff}}(u, t_0 + \Delta t|u_0, h, t_0) p_U(u_0, t_0) p_H(h, t_0 + \Delta t) \quad (\text{S45})$$

Since we are considering small  $\Delta t$  (with respect to  $\tau_H \sim \tau_U$ ), we can employ an additional simplification to compute the propagator  $P_U^{\text{eff}}$ . As before, we consider only the transitions between nearest neighbors in the  $U$  space. In other words, the reduced space on which we need to calculate the propagator is  $(u_0 - 1, u_0, u_0 + 1)$ . It is obtained solving the following Master Equation (using only  $P$  for simplicity of notation):

$$\partial_t P(u|u_0, h) = W^{\text{nn}} P(u|u_0) \quad (\text{S46})$$

with the transition matrix:

$$\begin{aligned} W_{12}^{\text{nn}} &= \hat{W}_{u_0 \rightarrow u_0-1} = \Gamma_0^U u_0 & W_{13}^{\text{nn}} &= \hat{W}_{u_0+1 \rightarrow u_0-1} = 0 \\ W_{21}^{\text{nn}} &= \hat{W}_{u_0-1 \rightarrow u_0} = \Gamma_{u_0-1 \rightarrow u_0}^{\text{eff}} & W_{23}^{\text{nn}} &= \hat{W}_{u_0+1 \rightarrow u_0} = \Gamma_0^U (u_0 + 1) \\ W_{31}^{\text{nn}} &= \hat{W}_{u_0+1 \rightarrow u_0-1} = 0 & W_{32}^{\text{nn}} &= \hat{W}_{u_0 \rightarrow u_0+1} = \Gamma_{u_0 \rightarrow u_0+1}^{\text{eff}} \end{aligned}$$

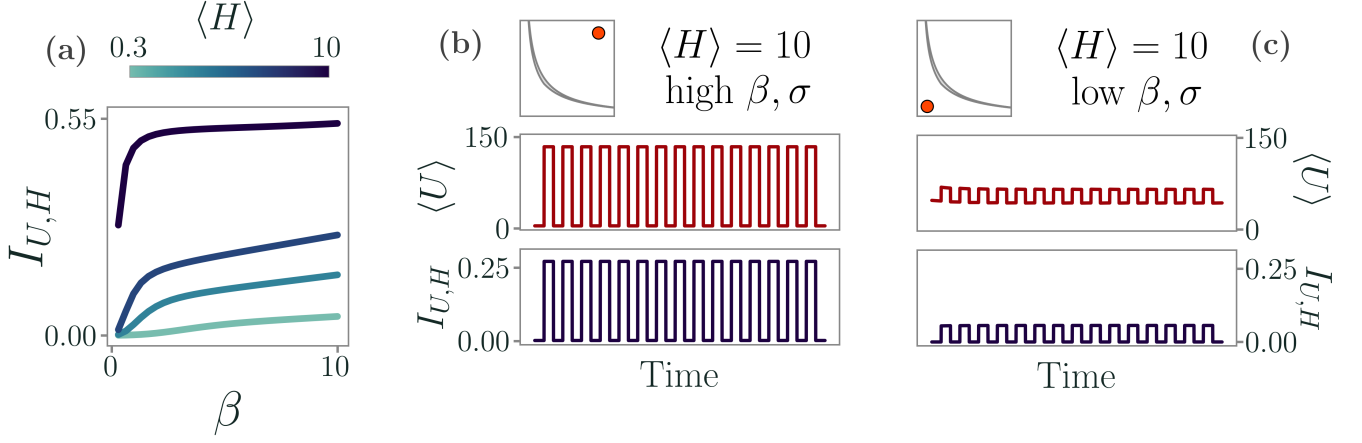


FIG. S1. Effects of the external signal strength and thermal noise level on sensing. (a) At fixed and low  $\sigma = 0.1$  and constant exponentially distributed signal with mean  $\langle H \rangle$ . As  $\langle H \rangle$  decreases, the system captures less information and it needs to operate at lower temperatures to sense the signal. In particular, as the temperature decreases,  $I_{U,H}$  becomes larger. (b) In the dynamical case, outside the optimal surface, at high  $\beta$  and high  $\sigma$ , storage is not produced and thus no negative feedback is present. The system does not display adaptation, and  $I_{U,H}$  is smaller than inside the optimal surface (gray area). (c) In the opposite regime, at low  $\beta$  and  $\sigma$ , the system is dominated by thermal noise. As a consequence, the average readout  $\langle U \rangle$  is high even when the external signal is not present ( $\langle H \rangle = \langle H \rangle_{\min} = 0.1$ ), and it captures only a small amount of information  $I_{U,H}$ , which is masked by thermal activations. Other simulation parameters for this figure are  $\langle U \rangle_A = 150$ ,  $\langle U \rangle_P = 0.5$ ,  $\alpha = 2/3$ , and  $\Gamma_S^0 = 1 = \Delta E = g$ . For the dynamical case,  $T_{\text{on}} = T_{\text{off}} = 100\Delta t$ .

the diagonal is fixed to satisfy the conservation of normalization, as usual. The solution is:

$$P(u|u_0, h) = p_{U|H}^{\text{st}} + \sum_{\nu} w_{\nu} a^{(\nu)} e^{\lambda_{\nu} \Delta t} \quad (\text{S47})$$

where  $w_{\nu}$  and  $\lambda_{\nu}$  are respectively eigenvectors and eigenvalues of the transition matrix  $W^{\text{nn}}$ . The coefficients  $a^{(\nu)}$  have to be evaluated according to the condition at time  $t_0$ :

$$P_{U|H}(u|u_0, h) = p_{U|H}^{\text{st}} + \sum_{\nu} w_{\nu} a^{(\nu)} = \delta_{u, u_0} \quad (\text{S48})$$

where  $\delta_{u, u_0}$  is the Kroenecker's delta. To evaluate the information content of this model, we also need:

$$\begin{aligned} p_U(u, t_0 + \Delta t) &= \sum_{u_0} p_U(u_0, t_0) \int dh P_U^{\text{eff}}(u, t_0 + \Delta t | u_0, h, t_0) p_H(h, t_0 + \Delta t) \\ p_{U|H}(u, t_0 + \Delta t | h) &= \sum_{u_0} P_U^{\text{eff}}(u, t_0 + \Delta t | u_0, h, t_0) p_U(u_0, t_0) \end{aligned} \quad (\text{S49})$$

Notice that the knowledge of  $p_U$  is necessary to evaluate  $p_{U|H}$ .

It is straightforward to figure out why a direct feedback from  $U$ , with this population undergoing a slow dynamics, cannot lead to an adaptive response. Indeed, at a fixed distribution of the external signal, the stationary solution of  $\langle U \rangle$  is given and takes into account the effect of the negative feedback. Hence, if the system starts with a very low readout population (no signal), the dynamics induced by a switching signal can only bring  $\langle U \rangle$  to its steady state with intervals in which the population will grow and intervals in which it decreases. Naively speaking,  $\langle U \rangle$  behaves as the storage in the complete model, since it is actually playing the same role of storing information in this simplified context. Manifestly, this is not an adaptation dynamics. By simulating Eq. (S49), we obtain the same result.

## SV. INFORMATION DYNAMICS AND MODEL PARAMETERS

### A. Effects of the external signal strength and thermal noise level

In the main text, for analytical ease, we take the environment to be an exponentially distributed signal,

$$p_H(h, t) = \lambda(t) e^{-h\lambda(t)} \quad (\text{S50})$$

where  $\lambda$  is its inverse characteristic scale. In particular, we describe the case in which no signal is present by setting  $\lambda$  to be large, so that the typical realizations of  $H$  would be too small to activate the receptors. On the other hand, when  $\lambda$  is small, the values of  $h$  appearing in the rates of the model are large enough to activate the receptor and thus allow the system to sense the signal.

In the dynamical case, we take  $\lambda(t)$  to be a square wave, so that  $\langle H \rangle = 1/\lambda$  alternates between two values  $\langle H \rangle_{\min}$  and  $\langle H \rangle_{\max}$ . We denote with  $T_{\text{on}}$  the duration of  $\langle H \rangle_{\max}$ , and with  $T_{\text{off}}$  the one of  $\langle H \rangle_{\min}$ . In practice, this signal mimics an on-off dynamics, where the stochastic signal is present only when its average is large enough,  $\langle H \rangle_{\max}$ . In the main text, we take  $\langle H \rangle_{\min} = 0.1$  and  $\langle H \rangle_{\max} = 10$ , with  $T_{\text{on}} = T_{\text{off}} = 100\Delta t$ .

In Figure S1a we study the behavior of the model in the presence of a static exponential signal, with average  $\langle H \rangle$ . We focus on the case of low  $\sigma$ , so that the production of storage is favored. As  $\langle H \rangle$  decreases,  $I_{U,H}$  decreases as well. Hence, as expected, information acquired through sensing depends on the strength of the external signal that coincides with the energy input driving receptor activation. However, the system does not display for all parameters an emergent information dynamics, memory, and adaptation. In Figure S1b we see that, when the temperature is low but  $\sigma$  is high, the system does not adapt and  $\Delta I_{U,H} = 0$ . On the other hand, when thermal noise dominates (Figure S1c) even when the external signal is small, the system produces a large readout population due to random thermal activation. As a consequence, it cannot sense the external signal even when it is present, and  $I_{U,H}$  is always small. It is important to remind here that, as we see in the main text in Figure 3b, at fixed  $\sigma$  and as a function of  $\beta$ ,  $I_{U,H}$  is not monotonic. This is due to the fact that low temperatures typically favor sensing and adaptation, but they also intrinsically suppress readout production. Thus, at high  $\beta$ ,  $\sigma$  needs to be small to effectively store information. In doing so, the system can capture more information - as thermal noise is negligible - but dissipate energy. Vice versa, a small  $\sigma$  is detrimental at high temperatures since the system produces storage as a consequence of thermal noise. This complex interplay is captured by the Pareto-like optimization, which gives us an effective relation between  $\beta$  and  $\sigma$  to maximize storage while minimizing dissipation.

## B. Static and dynamical optimality

In Figure S2, we plot the average readout population,  $\langle U \rangle$ , the average storage population,  $\langle S \rangle$ , the mutual information between them,  $I_{U,S}$ , and the entropy production of the internal processes,  $\dot{\Sigma}_{\text{int}}$ , as a function of  $\beta$  and  $\sigma$  and in the presence of a static field. The optimal values of  $\beta$  and  $\sigma$  obtained by minimizing the Pareto-like functional

$$\mathcal{L}(\beta, \sigma) = \gamma_1 \frac{I_{U,H}(\beta, \sigma)}{\max(I_{U,H})} + \gamma_2 \frac{\Delta I_f(\beta, \sigma)}{\max(\Delta I_f)} - (1 - \gamma_1 - \gamma_2) \frac{\delta Q_R(\beta, \sigma)}{\max(\delta Q_R)}, \quad \gamma_1 + \gamma_2 = 1,$$

are such that both  $\langle U \rangle$  and  $\langle S \rangle$  attain intermediate values. Thus, large/small production of readout/storage is detrimental to sensing. Similar considerations can be drawn for the dissipation of internal processes,  $\dot{\Sigma}_{\text{int}}$ . Interestingly, the dependence between readout and storage, quantified by the mutual information  $I_{U,S}$ , is not maximized at optimality. This suggests that excessively strong negative feedback impedes information, while promoting dissipation in the receptor,  $\delta Q_R$ , thus being suboptimal.

In Figure S3, we study the dynamical behavior of the model under a repeated external signal, as in Figure 3f-g-h in the main text. In particular, given an observable  $O$ , we define its change under a repeated signal  $\Delta O$  as the difference between the maximal response to the signal at large times and the maximal response to the first signal (Figure S3a). In Figure S3b we see in particular that  $\Delta \langle U \rangle$  is maximal in the region where the change in information feedback  $\Delta \Delta I_f$  is negative, suggesting that a strong adaptation fueled by a large storage concentration is ultimately detrimental for information processing. Furthermore, in this region the entropy produced by internal processes,  $\dot{\Sigma}_{\text{int}}$ , is maximal.

## C. Interplay between information storage and signal duration

In the main text and insofar, we have always considered the case  $T_{\text{on}} = T_{\text{off}}$ . We now study the effect of the signal duration and the pause length on sensing (Figure S4). If the system only receives short signals between long pauses, the slow storage build-up does not reach a high level of concentration. As a consequence, the negative feedback on the receptor is less effective and adaptation is suppressed (Figure S4a). Therefore, the peak of  $\Delta I_{U,H}$  in the  $(\beta, \sigma)$  plane takes place below the optimal surface, as  $\sigma$  needs to be smaller than in the static case to boost storage production during the brief periods in which the signal is present. On the other hand, in Figure S4b we consider the case of a long signal with short pauses. In this scenario, the slow dynamical evolution of the storage can reach large concentrations at larger values of  $\sigma$ , thus moving the optimal dynamical region slightly above the Pareto-like surface.

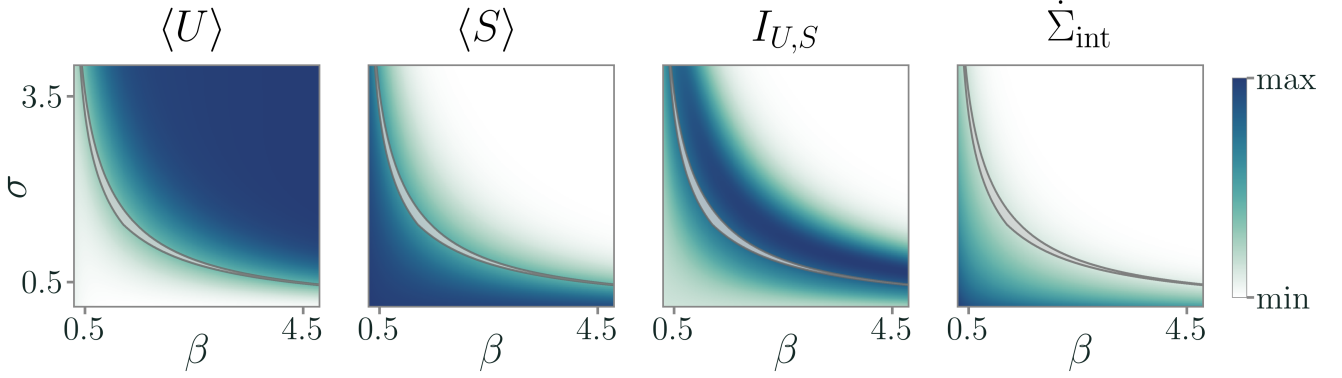


FIG. S2. Behavior of the average readout population,  $\langle U \rangle$ , the average storage population,  $\langle S \rangle$ , the mutual information between them,  $I_{U,S}$ , and the entropy production of the internal processes,  $\dot{\Sigma}_{\text{int}}$ , as a function of  $\beta$  and  $\sigma$  and in the presence of a static field. The gray area represents the Pareto-like optimal surface. The signal is exponentially distributed with an inverse characteristic scale  $\lambda = 0.1$ , so that  $\langle H \rangle = 10$ . Other simulation parameters are as in Figure S1.

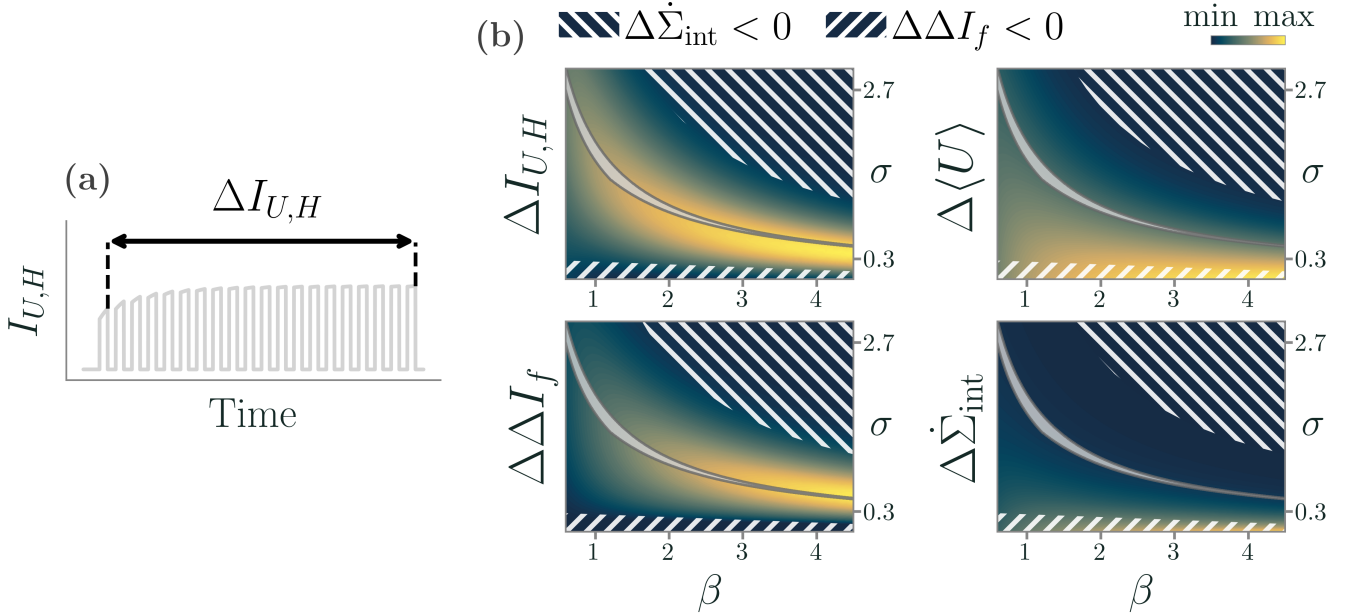


FIG. S3. Dynamical optimality under a repeated external signal. (a) Schematic definition of how we study the dynamical evolution of relevant observables, by comparing the maximal response to a first signal with the one to a signal at large times. (b) Behavior of the increase in readout information,  $\Delta I_{U,H}$ , in feedback information,  $\Delta \Delta I_f$ , in average storage population,  $\Delta \langle U \rangle$ , and in entropy production,  $\Delta \dot{\Sigma}_{\text{int}}$ . The gray area represents the Pareto-like optimal surface in the presence of a static field. Simulation parameters are as in Figure S1. In particular, recall the signal is exponentially distributed whose characteristic scale follows a square wave, with  $\langle H \rangle_{\text{max}} = 10$ ,  $\langle H \rangle_{\text{min}} = 0.1$ , and  $T_{\text{on}} = T_{\text{off}} = 100\Delta t$ .

## SVI. EXPERIMENTAL SETUP

Acquisitions of the zebrafish brain activity were carried out in *Elavl3:H2BGCaMP6s* larvae at 5 days post fertilization raised at  $28^\circ\text{C}$  on a 12 h light/12 h dark cycle according to the approval by the Ethical Committee of the University of Padua (61/2020 dal Maschio). Larvae were embedded in 2 percent agarose gel and their brain activity was recorded using a multiphoton system with a custom 3D volumetric acquisition module. Briefly, the imaging path is based on an 8-kHz galvo-resonant commercial 2P design (Bergamo I Series, Thorlabs, Newton, NJ, United States) coupled to a Ti:Sapphire source (Chameleon Ultra II, Coherent) tuned to 920nm for imaging GCaMP6 signals and modulated by a Pockels cell (Conoptics). The fluorescence collection path includes a 705 nm long-pass main

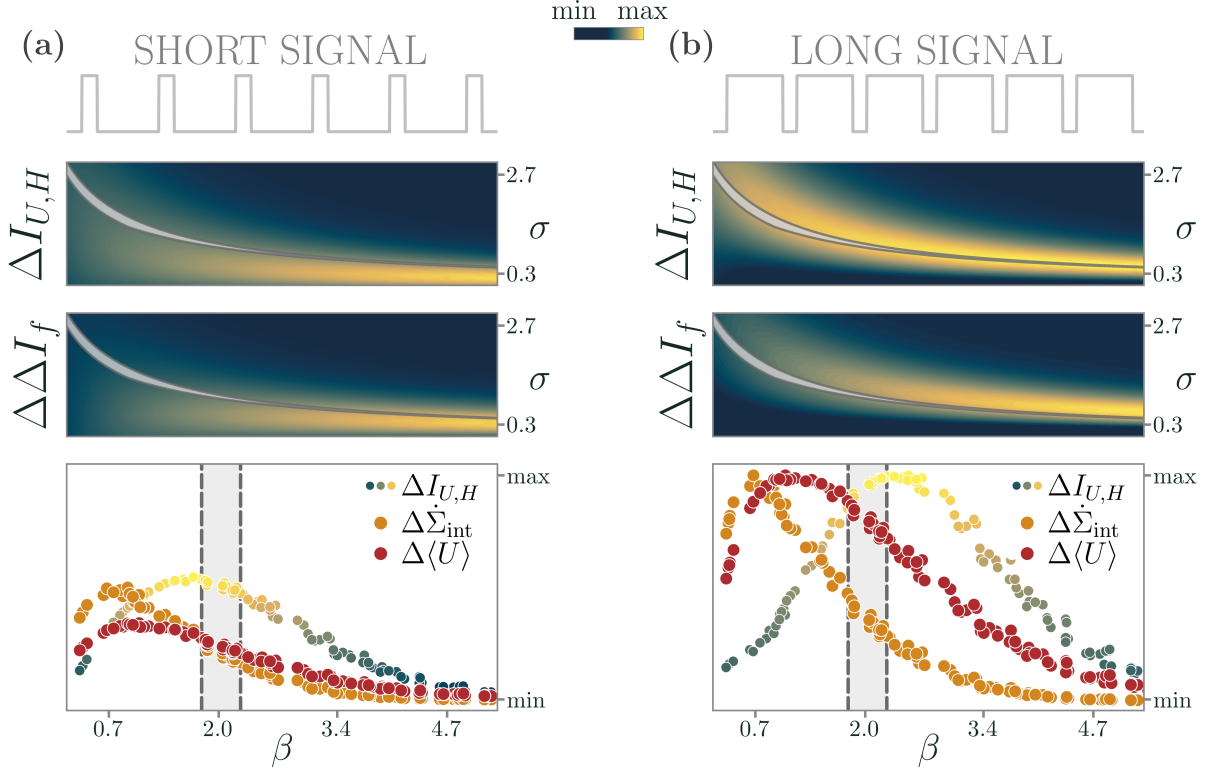


FIG. S4. Effect of the signal duration on sensing. (a) If the system only receives the signal for a short time ( $T_{\text{on}} = 50\Delta T < T_{\text{off}} = 200\Delta T$ ) it does not have enough time to reach a high level of storage concentration. As a consequence, both  $\Delta U$  and  $\Delta I_{U,H}$  are smaller, and thus adaptation is less effective. (b) If the system receives long signals with brief pauses ( $T_{\text{on}} = 200\Delta T > T_{\text{off}} = 50\Delta T$ ), instead, the adaptation mechanisms promote information storage and thus readout adaptation. Other simulation parameters are as in Figure S3.

dichroic and a 495nm long-pass dichroic mirror transmitting the fluorescence light toward a GaAsP PMT detector (H7422PA-40, Hamamatsu) equipped with EM525/50 emission filter. Data were acquired at 30 frames per second, using a water dipping Nikon CFI75 LWD 16X W objective covering an effective field of view of about  $450 \times 900\mu\text{m}$  with a resolution of  $512 \times 1024$  pixels. The volumetric module is based on an electrically tunable lens (Optotune) moving continuously according to a saw-tooth waveform synchronized with the frame acquisition trigger. An entire volume of about  $180 - 200\mu\text{m}$  in thickness encompassing 30 planes separated by about  $7\mu\text{m}$  is acquired at a rate of 1 volume per second, sufficient to track the relative slow dynamics associated with the fluorescence-based activity reporter GCaMP6s.

As for the visual stimulation, looming stimuli were generated using Stytra and presented monocularly on a  $50 \times 50\text{mm}$  screen using a DPL4500 projector by Texas Instruments. The dark looming dot was presented 10 times with 150s interval, centered with the fish eye and with a  $1/v$  parameter of 8.3 s, reaching at the end of the stimulation a visual angle of  $79.4^\circ$  corresponding to an angular expansion rate of  $9.5^\circ/\text{s}$ . The acquired temporal series were first processed using an automatic pipeline, including motion artifact correction, temporal filtering with a rectangular window 3 second long, and automatic segmentation using Suite2P. Then, the obtained dataset was manually curated to resolve segmentation errors or to integrate cells not detected automatically. We fit the activity profiles of about 52,000 cells with a linear regression model (scikit-learn Python Library) using a set of base functions representing the expected responses to each of the stimulation events, obtained convolving an exponentially decaying kernel of the GCaMP signal lifetime with square waveforms characterized by an amplitude different from zero only during the presentation of the corresponding visual stimulus. The resulting coefficients were divided for the mean squared error of the fit to obtain a set of scores. The cells, whose score fell within the top 5 of the distribution, were considered for the dimensionality reduction analysis.

The resulting fluorescence signals  $F^{(i)}$ , for  $i = 1, \dots, N_{\text{cells}}$ , were processed by removing a moving baseline to account for baseline drifting and fast oscillatory noise [56]. Briefly, for each time point  $t$ , we selected a window  $[t - \tau_2, t]$  and

evaluated the minimum smoothed fluorescence,

$$F_0^{(i)} = \min_{u \in [t-\tau_2, t]} \left[ \frac{1}{\tau_1} \int_{u-\tau_1/2}^{u+\tau_1/2} F(s) ds \right]. \quad (\text{S51})$$

Then, the relative change in fluorescence signal,

$$R^{(i)}(t) = \frac{F^{(i)}(t) - F_0^{(i)}}{F_0^{(i)}} \quad (\text{S52})$$

is smoothed with an exponential moving average. Thus, the neural activity profile for the  $i$ -th cell that we use in the main text is given by

$$x^{(i)}(t) = \frac{\int_0^t R(t-\tau)w(\tau)d\tau}{\int_0^t w(\tau)d\tau}, \quad w(t) = \exp\left[-\frac{t}{\tau_0}\right]. \quad (\text{S53})$$

In accordance with the previous literature [56], we set  $\tau_0 = 0.2$  s,  $\tau_1 = 0.75$  s, and  $\tau_2 = 3$  s. The qualitative nature of the low-dimensional activity in the PCA space is not altered by other sensible choices of these parameters.

---